WILEY-VCH

DOI: 10.1002/smll.201703539

Article type: Full Paper

Title: Endolysosomal-Escape Nanovaccines through adjuvant-induced tumor antigen assembly for enhanced effector $CD8^+$ T cell activation

Liping Qiu, Michael Valente, Yusuf Dolen, Eliezer Jäger, Martin ter Beest, Liyan Zheng, Carl G. Figdor and Martijn Verdoes**

Dr. L. Qiu, L. Zheng

Molecular Science and Biomedicine Laboratory, State Key Laboratory of Chemo/Biosensing and Chemometrics, College of Chemistry and Chemical Engineering, Hunan University, Changsha, 410082, China

Dr. L. Qiu, Dr. M. Valente, Dr. Y. Dolen, Dr. E. Jäger, Dr. M. Beest, Prof. C. Figdor, Dr. M. Verdoes.

Department of Tumor Immunology, Institute for Molecular Life Sciences, Radboud University Medical Center, Nijmegen, the Netherlands.

E-mail: Carl.Figdor@radboudumc.nl; Martijn.Verdoes@radboudumc.nl

Keywords: cancer nanovaccines, T cell activation, cross-presentation, endolysosomal escape, antigen/adjuvant codelivery

Abstract: The activation of tumor-specific effector immune cells is key for successful immunotherapy and vaccination is a powerful strategy to induce such adaptive immune responses. However, the generation of effective anti-cancer vaccines is challenging. To overcome these challenges, we develop a novel straight-forward strategy of adjuvant-induced tumor antigen assembly to generate nanovaccines with superior antigen/adjuvant loading efficiency. To protect nanovaccines in circulation and to introduce additional functionalities, a biocompatible polyphenol coating is installed. The resulting functionalizable nanovaccines are equipped with a pH (low) insertion peptide (pHLIP) to facilitate endolysosomal escape and to promote cytoplasmic localization, with the aim to enhance cross-presentation of the antigen by dendritic cells to effectively activate $CD8^+$ T cell. Our results demonstrate that pHLIP-functionalized model nanovaccine can induce endolysosomal escape and enhance $CD8^+$ T cell activation both *in vitro* and *in vivo*. Furthermore, based on the adjuvant-induced antigen assembly, nanovaccines of the clinically relevant tumor-associated antigen NY-ESO-1 are generated and show excellent capacity to elicit NY-ESO-1-specific $CD8^+$ T cell activation, demonstrating a high potential of this functionalizable nanovaccine formulation strategy for clinical applications.

1. Introduction

Cytotoxic $CD8^+$ T cells are a crucial component of the adaptive immune system and contribute significantly in immune defense against neoplastic and infected cells.[1] Recent clinical breakthroughs in cancer therapy are specifically aimed at inducing and enhancing a potent and long-lasting $CD8^+$ T cell response against tumors.[2] Cancer vaccination is a clinically attractive strategy for anti-tumor T cell activation due to its intrinsic specificity, lack of major toxicities and long-term immunological memory. Dendritic cells, the most

professional antigen-presenting cells that connect innate immunity with adaptive immunity, play a central role in vaccination.[3,4] *Ex vivo*-generated DC vaccines pulsed with tumor-associated antigens show promising results in preliminary clinical trials, but these vaccine preparation processes for each individual patient require specialized GMP facilities, equipment and trained personnel and may affect DC viability and migratory capacity, thus hampering widespread clinical application.[5] Therefore, alternative vaccination strategies that directly pulse DCs with tumor-associated antigens *in vivo* would be more suitable for clinical practice, and more importantly, would exploit the native migratory capacity of DCs.[6,7]

Meanwhile, vaccination with tumor-associated antigens alone results in poor immune responses. To amplify and to steer immunogenicity, coadministration of immunostimulatory adjuvants, such as lipo-polysaccharide (LPS, an amphiphilic Toll-like receptor 4 ligand), have been used.[8,9] It was reported that the timing of antigen and adjuvant encounter by DCs has significant impact on the outcome of the immune response.[10] Particulate packages of antigens and adjuvants, mimicking natural pathogens, have been shown to maximize the immune activation through enhanced antigen presentation efficiency of DCs.[11] Many particulate vaccine delivery systems have been developed through entrapping, encapsulating and attaching both antigens and adjuvants to the nanocarriers.[11-13] Despite the ability to induce DC-mediated T cell activation, most of these nanovaccines are limited in their clinical applications because of low antigen/adjuvant loading efficiency, complicated preparation, and involvement of toxic materials or solvents. Therefore, alternative strategies with simple design, convenient operation, high biocompatibility and high antigen/adjuvant loading efficiency are being sought.

After uptake and processing by DCs, exogenous antigens generally end up in the major histocompatibilty complex (MHC) class II presentation pathway, resulting in the activation of $CD4^+$ T helper cells. A loophole process termed cross-presentation enables the presentation of

exogenous antigens in the context of MHC class I to activate $CD8^+$ cytotoxic T cells.[14,15] Several pathways have been suggested for cross-presentation, of which the cytosolic pathway is the most widely accepted. A key step in this pathway is the endolysosomal escape of the antigen to the cytoplasm and its subsequent processing by the proteasome and peptidases before transport by the transporter associated with antigen processing (TAP) and loading of the resulting peptide epitopes onto MHC I molecules.[14] Therefore, nanovaccine delivery systems that facilitate the escape of the antigens from endolysosome into the cytoplasm are expected to enhance DC cross-presentation and effectively stimulate $CD8^+$ T cell-based antitumor immunity.

Inspired by the nanoparticle albumin–bound paclitaxel formulation (Abraxane),[16-18] combined with the consideration that many antigens are albumin-like proteins and many immunostimulatory adjuvants are hydrophobic or amphiphilic molecules, we attempted to induce antigen assembly into nanoparticles by addition of adjuvants to generate nanovaccines (**Figure** 1A). To prevent cargo leakage in blood circulation and to introduce additional functionalities, an azide-functionalized biocompatible polyphenol coating[19] was installed on the surface of the nanovaccines. Subsequently, using click chemistry the polyphenol-coated nanovaccines were functionalized with pH (low) insertion peptides (pHLIP) capable of inducing translocation across the lipid bilayers in acidic environments, [20,21] with the aim to promote nanovaccine escape from the acidic endolysosomal pathway into the cytoplasm (Figure 1B). Such a vaccine design is expected to allow efficient codelivery of both antigen and adjuvant to DCs and enhance their cross-presentation capability to activate antigen-specific cytotoxic T cells. Finally, we applied this adjuvant-induced antigen assembly strategy to generate nanovaccines of a clinically relevant tumor-associated antigen, NY-ESO-1,[22] to assess the potential of this nanovaccine development strategy for clinical applications.

2. Results and Discussion

2.1 Adjuvant-induced antigen assembly

As a starting point for the co-assembly of antigen and adjuvant, we applied ovalbumin (OVA), a protein widely used for studying antigen-specific immune responses,[23] as a model antigen and LPS as an immunostimulatory adjuvant. Surprisingly, addition of LPS into an aqueous solution of OVA under moderate stirring induced OVA assembly into uniform spherical nanoparticles (91.0±10.1 nm), while we observed random protein aggregates in the absence of LPS (Figure 2A). Of note, the stirring treatment is critical for the formation of the nanoparticles, and no nanoparticles can be found by omitting this treatment (Figure S1). Presumably, stirring increases the kinetic energy and the number of collisions between reactant molecules enabling LPS to bind in the multiple hydrophobic binding domains in OVA and the organization into spherical nanoparticles, which are subsequently stabilized by LPS as surfactant. The LPS concentration dependency of nanoparticle formation was tested by titrating a 1 mg/mL OVA solution with LPS of different concentrations. The particle size showed a dose-dependent increase and reached a plateau at the LPS concentration of 10 μg/mL (Figure 1B, panel i). Meanwhile, the entrapment of LPS showed a dose-dependent linear increase, even after the particle size had plateaued (Figure 2B, panel ii). To obtain a high loading efficiency of OVA, the OVA-LPS nanoparticles prepared at the mass ratio of OVA:LPS = 1 mg:10 μg was used for the rest of the experiments.

The ability of LPS to induce assembly of two other albumins, bovine serum albumin (BSA) and sheep serum albumin (SSA), was also tested. Transmission electron microscopy (TEM) images showed both BSA and SSA (1 mg/mL) could assemble into uniform spherical nanoparticles upon addition of LPS (10 μg/mL), with particle size of 65.0±7.5 nm and 60.1±15.6 nm, respectively (Figure S2A and S2B) indicating that LPS could induce the

assembly of various albumins into nanoparticles. Our previous work demonstrated that co-encapsulation of OVA with α-galactosylceramide (αGalcer), a CD1d ligand capable of activating NKT cells, in PLGA nanoparticles could induce a highly potent anti-OVA $CD8^+$ T cell immune response *in vivo*.[24] To test the universality of our nanovaccine formation strategy, amphiphilic αGalcer was added to a stirred aqueous solution of OVA, and the resulting product was analyzed with TEM. As shown in Figure 2C, αGalcer (20 μg/mL) could induce OVA (1 mg/mL) assembly into spherical nanoparticles of 131.7±9.92 nm. Furthermore, nanovaccines were generated using the detoxified LPS-derivative monophosphoryl lipid A (MPLA).[25] Stirring of MPLA (10 μg/mL) with OVA (1 mg/mL) resulted in spherical nanoparticles of 103.4±22.0 nm (Figure 2D). These results suggest a widely applicable strategy for the generation of co-assembled antigen/adjuvant nanovaccines. More importantly, these nanovaccines were fabricated by simply stirring the mixture of antigen and adjuvant in phosphate buffered saline (PBS), with no need to involve additional carrier materials, organic solvents and complicated operations, offering a completely non-toxic and convenient nanovaccine development strategy with high cargo-loading efficiency.

2.2 Nanovaccine coating

In order to protect the antigen-adjuvant nanovaccines in circulation but also to equip them with functional moieties, a biocompatible and biodegradable polyphenol coating was installed on the particle surface. Polyphenols are a class of natural compounds abundantly found in plants and food, and show potential benefits for protecting the body from radiation damage and pathogen infection.[26,27] They can polymerize to generate a uniform polyphenol coating on the surface of various substrates in mildly alkaline aqueous solution.[19,28] In addition, the polyphenol coating can be biodegraded by glutathione (GSH) which is usually present in the millimolar range (0.5~10 mM) in the cytoplasm,[29] thus offering a strategy to promote the release of the vaccine content after cellular uptake. Moreover, by exploiting the capability of

polyphenols to covalently react with nucleophiles, such as amines and thiols, functional moieties can be easily introduced onto the NP surface.[19] Here, we chose epigallocatechin gallate (EGCG), [28] one of the typical polyphenol molecules, as a model precursor to perform the polyphenol coating. With treatment of EGCG in PBS (pH 7.8) at room temperature for 1 hour, an obvious polyphenol coating was observed covering the nanoparticle surface (Figure 3A). The particle size increased from 91.0±10.1 nm (Figure 2A) to 123.1±15.7 nm (Figure 3A, panel i), indicating a coating layer thickness of about 16 nm. The GSH-dependent polyphenol coating degradation was determined via a dye leakage experiment. To detect a fluorescent signal that indicates the cargo release event, the fluorescent dye ATTO-647 was incorporated into the OVA-LPS nanoparticles. The release kinetics of ATTO-647 from polyphenol-coated nanoparticles was studied at different GSH concentrations. In the absence of GSH, the release of ATTO-647 from nanoparticles was rather slow, with less than 20% release of the entire payload after 80 h, indicating a high stability of the EGCG-coated nanoparticle (Figure 3B). A higher dye release rate was obtained when increasing the GSH concentration, and over 78% of dyes was released after incubation in 10 mM GSH for 80 h, indicating a GSH-responsive biodegradation of the polyphenol-coated NPs. In addition, the coating strength was adjusted by changing the incubation time of nanoparticles in the EGCG solution. A slower cargo release profile was obtained with a longer polyphenol coating time (Figure S3). After phagocytosis, the nanovaccines enter the endocytic pathway where endocytic compartments gradually acidify upon maturation. Hence, the stability of polyphenol-coated particles in acidic environment was compared to that at physiological pH. The release kinetics increased from about 12% release of the entire payload after 48 h to some 27% at lower pH (Figure S4). This partial pH dependent cargo release could play an important role in adjuvant receptor engagement. The ability of our nanoparticles to induce DC maturation and the impact of the polyphenol coating thereon was studied by incubating two types of murine bone marrow derived DCs (GM-CSF BMDCs and $CD103^+$ BMDCs) with

four OVA-LPS nanoparticles of different polyphenol coating strengths. As indicated by the expression of MHC II and the co-stimulatory molecules CD80 and CD40,[30] our antigen-adjuvant nanoparticles were able to induce robust DC maturation. Slower DC maturation was induced by the nanoparticle with stronger polyphenol coatings, correlating with the release kinetics (Figure S5). To strike a balance between protection and immune stimulation, the OVA-LPS nanoparticles coated with polyphenol for 1 hour (termed as NPs) was chosen for the rest of study. Of note, negligible impact of polyphenol on DC viability was observed (Figure S6), indicating excellent biocompatibility of these polyphenol-coated nanovaccines.

2.3 Coated nanovaccine functionalization with endolysosomal-escape peptide

The escape of exogeneous antigens from the endolysosomal pathway into the cytoplasm is one of the major mechanisms to enhance their cross-presentation onto MHC class I complexes to activate cytotoxic $CD8^+$ T cells. In efforts to facilitate nanovaccine escape from endolysosome, a pH (low) insertion peptide (pHLIP) [21] was applied to functionalize the NPs. As demonstrated by previous works, pHLIP is a pH-sensitive peptide, which remains unstructured at neutral and basic pHs.[31] However, in acidic environment, pHLIP switches into a rigid helical structure with its N-terminus rapidly inserting into phospholipid bilayers, and subsequently translocates its C-terminus across cell membranes. Since endolysosome are acidified vesicles with a low pH ranging from 4.5 to 6.5, we hypothesized that pHLIP could enable the nanovaccine escape into the slightly basic cytosol (pH 7.2).

During the oxidative EGCG polymerization process, quinones are formed, which were reacted with cysteine in a Michael-type fashion.[32] The resulting cysteine conjugates were then condensed with azido-pentaethylene glycol-amine to obtain azide-functionalized nanovaccines. These versatile intermediates can be decorated with various functional molecules using azide–alkyne click chemistry. Successful covalent modification of the azido-

NPs with alkyne-pHLIP was demonstrated by the reduced NP zeta potential (from -24.8±0.7 to -31.3±1.1), matching well with the negative charge of this peptide. Meanwhile, rather slight zeta potential change (0.7±1.0) was obtained when adding a control pHLIP having no alkyne-reactive group, indicating negligible random absorption of this peptide on the NP surface. Nanovaccines grafted with an alkyne-tagged control peptide, which has similar chemical properties as pHLIP but with no pH-dependent membrane translocation capability, were also synthesized and termed as NP-ctrl. In addition, as demonstrated by cytotoxicity assays (Figure S7) and DC maturation assays (including cell phenotype change and cytokine IL-12 production, Figure S8), the functionalization of the NPs with both pHLIP and control peptide has little influence on the biocompatibility and immune stimulation capability of the nanovaccines.

2.4 Cellular uptake and distribution

After successful synthesis and characterization of these nanovaccines, we next studied their cellular uptake and intracellular distribution. In order to detect a fluorescent signal that indicates the localization of the nanovaccines, OVA was covalently modified with ATTO-647 dyes, and fluorescent nanovaccines were generated using the aforementioned protocol. To demonstrate the pH-dependent membrane translocation of NP-pHLIP, a DC cell line, JAWS II, was incubated with the different fluorescent nanovaccines in phosphate buffer of different pH values for 1 hour and then analyzed by flow cytometry. The cellular uptake of NP-pHLIP was improved by acidification of the incubation buffer, while little difference was observed in the case of NP-ctrls (Figure 4A). Of note, at pH 7.4, the fluorescence signal from the cells incubated with NP-pHLIP was similar to that from the cells incubated with NP-ctrls, revealing a comparable cellular internalization capability of NP-pHLIPs and NP-ctrls in neutral environments. The pH-dependent cellular uptake of NP-pHLIPs was also visualized

with confocal laser scanning microscopy (CLSM) and confirmed by fluorescence intensity calculation (Figure S9).

To test whether NP-pHLIPs can escape from the endolysosomal pathway, DCs were incubated with fluorescent NPs, NP-ctrls or NP-pHLIPs for 7 hours, and subsequently imaged with CLSM in the presence of lysotracker green. An obvious colocalization of lysotracker signal and ATTO-647 signal was observed in the cells incubated with either NP-ctrls or NPs, with a Pearson's Coefficient higher than 0.78 in both cases (Figure 4B and 4C). In sharp contrast, NP-pHLIPs were found to be more excluded from lysotracker-stained compartments, as indicated by a Pearson's Coefficient of 0.53. Moreover, this difference can be extended to later time points (e.g., 30 hour), where similar observations were made (Figure S10). The intracellular distribution of NP-pHLIPs were also confirmed by immunostainings for LAMP1, a lysosomal marker protein. As shown in Figure 4D and 4E, colocalization of LAMP1 with NP-pHLIPs (Pearson's Coefficient=0.56) was lower than that with NP-ctrls (Pearson's Coefficient=0.73), further demonstrating pHLIP-facilitated lysosomal escape of the NPs. Early endosomal localization of NP-pHLIPs was also excluded by the low colocalization between NP-pHLIPs and the early endosomal protein marker, EEA1 ((Pearson's Coefficient=0.35, Figure S11). To quantify the cytoplasmic distribution of the nanovaccines, cytosol was extracted using a digitonin-based strategy,[33] and was proven to be free from contaminations of lysosome and endosome by Western Blotting (Figure S12). The OVA-ATTO-647 fluorescence of both cytosol and whole-cell lysate was measured by fluorescence spectrometry. The percentage of fluorescent OVA present in the cytosol of the cells incubated with NP-pHLIPs was about two-fold higher than that of the cells incubated with NP-ctrls (Figure 4F). Together, these results demonstrate for the first time that functionalization of NPs with pHLIP reduces their localization in lysosomes and promotes the translocation of the nanovaccines from the endolysosomal pathway into the cytoplasm.

2.5 *In vitro* cross-priming $CD8^+$ T cells

Having demonstrated the feasibility of NP-pHLIPs to escape from the lysosome and translocate to the cytoplasm, we proceeded to test whether these nanovaccines can enhance cross-presentation of antigens by DCs to efficiently prime $CD8^+$ T cells. Immature $CD103^+$ BMDCs were first incubated with the different vaccines for 24 hours. OVA-specific $CD8^+$ T cells harvested from OT-I transgenic mice (termed OT-I T cells)[34] were labeled with carboxyfluorescein diacetate succinimidyl ester (CFSE) and subsequently cocultured with the nanovaccine-treated DCs for 72 hours. CFSE dilution was measured by flow cytometry to evaluate OT-I T-cell proliferation (Figure 5A). The average number of cell divisions (termed as Mean cycles)[35] was calculated and is depicted in Figure 5B. The nanovaccine-pulsed DCs (both NP-pHLIP and NP-ctrl) can induce robust OT-I T cell proliferation in a dose-dependent manner, even at low OVA concentrations. Meanwhile, NP-pHLIPs show a tendency to induce stronger response than NP-ctrls. The efficacy differences between soluble OVA+LPS and the NPs were particularly striking at low vaccine doses. Specifically, at the OVA concentration of 0.4 μg/mL, OT-I proliferation (Mean cycles) induced by soluble OVA+LPS was only 0.05±0.12, which was about 41 and 52 times lower than that in the condition of equivalent NP-ctrls (2.04±0.14) and NP-pHLIPs (2.62±0.09), respectively (Figure 5B). Meanwhile, a much weaker OT-I T cell proliferation was caused by DCs pulsed with OVA only (Figure S13), indicating an important role of LPS in promoting DC-mediated immune responses.

Generating sufficient amounts of antigen-specific T cells is essential for effective anti-tumor immunotherapy. Furthermore, production of effector cytokines, including IL-2 and IFNy, are critical indicators for evaluating the activation status of T cells.[36,37] Similar to what was seen in the proliferation assay, the NP-ctrl and NP-pHLIP outperformed soluble OVA+LPS, with the biggest difference visible at the lower concentrations of antigen (Figure 5C and Figure S14). Here too, a stronger IL-2 and IFNy response was observed for the NP-

pHLIPs compared to NP-ctrls. The OVA-MPLA and OVA-αGalcer nanovaccines were also tested for their ability to enhance $CD103^+$ BMDCs induced in vitro OT-I T cell proliferation and IFNy production. The OVA-LPS nanovaccines alike, both these nanovaccines outperformed their respective soluble counterparts (Figure S15A, B). Furthermore, $CD103^+$ BMDCs incubated with the OVA-αGalcer nanovaccines were able to activate NKT cells more potently compare to soluble OVA+αGalcer as judged by the DN32.D3 NKT cell hybridoma activation assay,[38] indicating increased αGalcer presentation by CD1d (Figure S15C). Collectively, these results demonstrated that our nanovaccines dramatically increase the $CD8^+$ T cell priming efficiency of DCs compared to soluble vaccines.

2.6 *In vivo* cross-priming $CD8^+$ T cells and clinical perspectives

As initiation of a robust antigen-specific $CD8^+$ T cell response *in vivo* is our ultimate goal, we tested whether our nanovaccines can survive blood circulation and mount efficient OVA-specific $CD8^+$ T activation. Celltrace violet-labeled OT-I T cells were transferred into naïve C57Bl/6 mice which were then vaccinated with equivalent amounts of soluble OVA+LPS, NP-ctrls or NP-pHLIPs by intravenous injection. Three days after vaccination, these mice were sacrificed and OT-I T cell proliferation was assessed by flow cytometry. As shown in Figure 6, a significant enhancement of T cell proliferation was observed in both NP conditions, compared with that induced by soluble OVA+LPS. Meanwhile, between the NP vaccines, the pHLIP peptide-functionalized nanoparticle proved to be able to induce the greatest enhancement in T cell proliferation. These results confirm the capability of these functionalized nanovaccines to efficiently activate antigen-specific cytotoxic $CD8^+$ T cells *in vivo*. Although it is well established that tumor antigen specific T cell response correlates with (pre-)clinical outcome, future experiments using tumor-bearing animal models could be performed to further evaluate immunotherapeutic efficacy of these nanovaccines.

To further evaluate the potential of our nanovaccine generation strategy for clinical translation, a clinically relevant human tumor-associated antigen NY-ESO-1 was applied. Clinical studies where melanoma patients were treated with ipilimumab (anti-CTLA-4) demonstrated that those patients who showed a cytotoxic $CD8^+$ T cell response against NY-ESO-1 experienced more frequent clinical benefits compared to the patients without such a T cell response,[39] illustrating the need for efficient NY-ESO-1 vaccines. However, NY-ESO-1 is known to be hardly cross-presented by human monocyte-derived DCs (moDCs) in its native form, hindering the development of full-length NY-ESO-1-based cancer vaccines.[40] By using the nanovaccine generation strategy described above, spherical NY-ESO-1/LPS nanoparticles of 491.0±53.6 nm were generated (Figure 7A) and covered with a polyphenol coating. To test the ability of these nanovaccines to induce cross-priming of antigen specific T cells, human mo DCs were first incubated with either soluble NY-ESO-1+LPS, uncoated or polyphenol-coated NY-ESO-1/LPS nanoparticles for 24 hours. The antigen-pulsed moDCs were then co-incubated with autologous naïve $CD8^+$ T cells transfected with NY-ESO-1 (p157–165) specific T cell receptor mRNA (Figure S16). After 48-hour incubation, IFNy production was measured with ELISA. Poor T cell cross-priming was achieved by moDCs pulsed with NY-ESO-1+LPS in soluble form, as indicated by an almost undetectable IFNy production (Figure 7B). Remarkably, our NY-ESO-1/LPS nanoparticles, both with and without polyphenol coating, could induce efficient cross-presentation of the HLA-A2-restricted NY-ESO-1 (p157–165) epitope derived from native full-length NY-ESO-1 protein, which could be judged by the induction of significant IFNy secretion. Our results show a high potential of our adjuvant-induced antigen assembly strategy for the generation of nanovaccines for effective antitumor immunotherapy.

3. Conclusion

In summary, we have developed a novel nanovaccine generation strategy on the basis of adjuvant-induced antigen assembly into nanoparticles. Unlike conventional cancer nanovaccines constructed by entrapping, encapsulating and attaching both antigens and adjuvants to the nanocarriers, our nanovaccines were generated by simply stirring the mixture of antigen and adjuvant in PBS, with no need to involve toxic carrier materials, organic solvents and complicated operation, offering a convenient and completely non-toxic nanovaccine generation strategy with high cargo loading efficiency. Subsequently, a biocompatible and functionalizable polyphenol coating was installed on the surface of the antigen/adjuvant nanoparticles, enabling cargo protection in blood circulation and introduction of various functional ligands. In an effort to enhance $CD8^+$ T cell activation, a pH (low) insertion peptide (pHLIP) with capability of translocation across the phospholipid bilayer in low-pH environments, was installed onto the surface of the polyphenol-coated nanovaccines. With the introduction of pHLIP, our nanovaccine was able to induce antigen escape from the acidic endolysosome and translocalize into the cytoplasm. Of note, unlike other endolysosome-disruptive peptides, pHLIP does not affect the integrity of endolysosome, which is beneficial for maintain the viability of DCs. When reaching the cytoplasm, the antigen release was promoted on the basis of the GSH-responsive biodegradable property of the polyphenol coating, thus enhancing the access of antigens to the MHC class I processing pathway. Our *in vitro* and *in vivo* experiments demonstrated that these nanovaccines can enhance the cross-presentation capability of DCs to efficiently activate effector $CD8^+$ T cells. Furthermore, this nanovaccine generation strategy was successfully applied to the clinically relevant tumor-associated antigen NY-ESO-1. The generated NY-ESO-1/LPS nanoparticles could greatly enhance the notoriously difficult activation of NY-ESO-1-specific cytotoxic T cells using full-length NY-ESO-1 protein. All these results demonstrate a high potential of our adjuvant-induced antigen assembly strategy for the production of functionalizable nanovaccines for clinical translation.

4. Experimental Section

4.1 Synthesis of polyphenol-coated OVA-LPS, OVA-αGalcer and OVA-MPLA nanoparticles

For synthesis of OVA-LPS nanoparticles, OVA (1 mg) were mixed with LPS of a certain concentration (except as otherwise noted, 10 μg of LPS was used) in phosphate buffer saline (PBS, pH 7.4, 1 mL) under moderate stirring at 4 °C for 48 hours. Subsequently, the OVA-LPS mixture was purified by centrifuge at 15000 rpm for 3 min to get rid of big aggregation, followed by dialysis in PBS using a dialysis bag of 50K MWCO to remove soluble OVA and LPS. The resulting nanoparticles were characterized by TEM imaging.

To form a polyphenol coating on the nanoparticle surface, OVA-LPS nanoparticles were suspended in phosphate buffer (10 mM) of pH 7.8 containing epigallocatechin gallate (EGCG, Sigma, 0.2 mg/mL), and stirred mildly at room temperature (RT) for a certain length of time (except as otherwise noted, 1 hour was used). The polyphenol-coated OVA-LPS nanoparticles were immediately purified through dialysis in PBS with a Slide-A-Lyzer™ Dialysis Cassettes of 20K MWCO (Thermo Fisher Scientific). The polyphenol coating was characterized by TEM imaging. For the generation of the OVA-αGalcer and OVA-MPLA nanovaccines, the same procedure was followed using the indicated amounts of adjuvant.

4.2 Synthesis of polyphenol-coated NY-ESO-1/LPS nanoparticles

For synthesis of NY-ESO-1/LPS nanoparticles, NY-ESO-1 (0.5 mg/mL, 100 μL) was mixed with LPS (1 mg/mL, 50 μL), and then added with PBS (350 μL). The mixture was stirred under moderate stirring at 4 °C for 48 hours. After that, the resulting NY-ESO-1/LPS nanoparticles were purified through dialysis in PBS using a dialysis bag of 50K MWCO. The polyphenol coating of NY-ESO-1/LPS nanoparticles was conducted by following the same

protocol described above. For preparation of soluble NY-ESO-1+LPS, equivalent NY-ESO-1 and LPS were mixed and used directly.

4.3 Cargo release kinetics of polyphenol-coated nanoparticles.

To establish a fluorescent signal that indicated the cargo release from the polyphenol-coated OVA-LPS nanoparticles, an ATTO-647 dye was incorporated during the OVA-LPS nanoparticle formation. Except for the incorporation of ATTO-647, the fluorescent polyphenol-coated OVA-LPS nanoparticles were prepared by following the above-mentioned protocol. To test the impact of glutathione (GSH) on the cargo release, the fluorescent OVA-LPS nanoparticles (1 mL) with polyphenol coated for 1 hour was added to a Slide-A-Lyzer™ dialysis device (20K MWCO, Thermo Scientific), and the devices were immersed in PBS (45 mL) containing GSH (0 mM, 1 mM, 5 mM or 10 mM) in a 50-mL dialysis tube with gentle shaking at 37 °C. At each given time point, a aliquot of the dialysis solution (100 μL) was collected for ATTO-647 fluorescence measurement. After that, the collected solution was returned to the corresponding dialysis tube. To test the impact of the polyphenol coating strength on cargo release, the fluorescent OVA-LPS nanoparticles coated with polyphenol for 0 hour, 1 hour, 2 hours or 4 hours were prepared, and PBS containing GSH (5 mM) was used as the dialysis buffer. The experimental process was conducted as mentioned above.

4.4 Functionalization of polyphenol-coated OVA-LPS nanoparticles

The OVA-LPS nanoparticles prepared at the mass ratio of OVA:LPS = 1 mg:10 μg and subsequently coated with polyphenol for 1 hour was used for the rest experiments and termed as NPs. To introduce functional groups on NPs, cysteine (1 mM) was first added into a stirred aqueous NP solution (in PBS) and incubated at RT for 1 hour. In this way, the electrophilic sites on NP surface was blocked, and plentiful carboxyl groups were introduced. After dialysis to remove free cysteine, EDC (4 mg) and NHS (6 mg) were added to the cysteine-

blocked NPs in PBS. The reaction components were mixed well and reacted at RT for 15 min. Subsequently, Amine-PEG-Azide (N_3-PEG5000-NH_2, Sigma Aldrich, 10 μL) was added in and reacted at RT for 2 hours. After that, free N_3-PEG-NH_2 were removed by dialysis with a Slide-A-Lyzer™ Dialysis Cassettes of 20K MWCO (Thermo Fisher Scientific). In this way, azide groups were introduced on the NP surface. Then, an alkynyl-terminated pH (low) insertion peptide (pHLIP) with the sequence of "CEEQQPWAQYLELLFPTETLLLEWG"[21] and a control peptide (ctrl) with the sequence of "ACEEQEPEARYLKELEPTKTLELKL" were purchased from GeneScript (Hongkong) and dissolved in DMF. For the peptide functionalization, the peptide solution (pHLIP or ctrl, 10 mg/mL, 40 μL) was added into the resulting azide-functionalized NPs (1 mL). After vortex, ascorbic acid solution (100 mM, 3 μL) was added in. The mixture was well vortexed and then degassed with Nitrogen for 30 seconds. Subsequently, Copper (II)-TBTA (10 mM, 30 μL) in 50% DMF was added into the mixture. The reaction components were flushed with nitrogen, vortexed thoroughly and reacted at RT overnight. The resultant products (NP-pHLIP and NP-ctrl) were purified via dialysis.

OVA content in the nanoparticles was determined using Pierce™ BCA Protein Assay Kit combined with Compat-Able™ Protein Assay Preparation Reagent Kit (Thermo Fisher). LPS content in the nanoparticles was measured with Endpoint Chromogenic LAL Assays (Lonza).

4.5 Studying cell uptake and intracellular distribution of NPs with fluorescence imaging

To establish a fluorescent signal that indicates cell uptake and intracellular distribution of NPs, OVA was covalently labelled with ATTO 647-COOH (ATTO-TEC) via carbodiimide crosslinker chemistry. The fluorescent OVA-LPS nanoparticles were synthesized, installed

with polyphenol coating and functionalized with pHLIPs or ctrls by following the protocol as described above.

JAWS II, a DC line, was used as a model cell in this experiment. 1) For lysotracker staining assay, JAWS II cells were incubated with the fluorescent NPs in culture medium (MEM alpha with ribonucleosides, deoxyribonucleosides, L-glutamine (4 mM), sodium pyruvate (1 mM), murine GM-CSF (5 ng/mL) and fetal bovine serum (20%)) in a 35-mm confocal dish at 37 ^{o}C with 5% CO_2 for a certain length of time. After removal of free NPs, the cells were stained with 1/1000 diluted lysotracker Green (Invitrogen) for 7 min, washed with PBS for three times, and imaged with Confocal Laser Scanning Microscope (CLSM, Olympus, FluoView™ FV1000) with a 63× oil-immersion objective. 2) For intracellular protein marker staining, the glass coverslips were treated with poly(l-lysine) in fridge overnight and washed with PBS. JAWS II cells were seeded at 5×10^5 cells per slide and incubated in culture medium at 37 °C with 5% CO_2 for 1 h. The fluorescent NP-pHLIPs or NP-ctrls were added to the cells and incubated for 7 h. The cells were fixed with 4% paraformaldehyde at room temperature for 15 min. After being washed with PBS, the cells were permeabilized with 0.1% Triton-X100 in PBA (PBS containing 1% BSA and 0.1% sodium azide) for 5 min, washed 3 times with PBS, and then blocked with 1% bovine serum albumin (BSA) plus glycine (0.5 mg/mL) for 30 min. After that, the cells were incubated with the primary antibodies against LAMP-1 and EEA1 in fridge overnight, followed by species-matched secondary antibodies conjugated with Alexa Fluor 488 (Invitrogen) and phalloidin-488 (Invitrogen) at room temperature for 1 h. Finally, coverslips were mounted with Prolong Gold antifade (life technologies) and imaged with CLSM. The colocalization between the ATT0-647 signal and the endo/lysosomal indicators (lysotracker, LAMP-1 and EEA1) was statistically analyzed by measuring the Pearson's Coefficient using the ImageJ software with a colocalization plugin. 3) To test the OVA content in cytosol, JAWSII cells (10^7) were

separately incubated with NP-pHLIPs and NP-ctrls in culture medium (pH 7.4) for the indicated length of time. After removal of free NPs through centrifuge, the cell cytosol was extracted using a digitonin-based method [33], and whole cell lysate was used as a reference. The ATTO-647 fluorescence intensity of both cytosol and whole cell lysate were measured with fluorescence spectrophotometer, and their intensity ratio (cytosol:whole cell) was used to assess the cytoplasm transportation capability of the nanovaccines.

4.6 Culture of Dendritic Cells from mouse bone marrow cells

The murine DCs were prepared by following the reported protocol with slight modifications.[41] C57BL/6 mice were sacrificed, and their femur and tibia were harvested. The bone marrow was flushed out with culture medium (1640 RPMI medium plus 10% FCS, 1% glutamine, 1% Antibiotic-Antimycotic and 50 μM 2-Mercaptoethanol) and collected by centrifuge at 1500 rpm for 5 min. 1) For GM-CSF BMDCs preparation,[42] the obtained bone marrow cells ($4x10^6$) were plated out in Petridish (Greiner, 10 cm, 633185) at culture medium (13 mL) containing granulocyte–macrophage colony-stimulating factor (GM-CSF, Peprotech, 20 ng/mL), and cultured at 37 °C with 5% CO_2 for 4 days. Subsequently, fresh culture medium (4 mL) containing GM-CSF (37.2 ng/mL) was added, and the cells were cultured for another 3 days. The resulting non-adherent cells (day 6) were harvested and resuspended in fresh culture medium containing GM-CSF (8,75 ng/mL) for further DC maturation assays. 2) For $CD103^+$ DCs preparation,[43] the obtained bone marrow cells (15×10^6/10 mL) were plated out in Petridish (Greiner, 10 cm, 633185) at culture medium (1640 RPMI medium plus 10% FCS and 1% 2-ME) containing fetal liver tyrosine kinase 3-Ligand (Flt3-L, 200 ng/mL) and GM-CSF (5 ng/mL), and cultured at 37 °C with 10% CO_2 for 5 days. Then, the cells were supplemented with complete medium (5 mL culture medium plus Flt3-L and GM-CSF) and further cultured for 4 days. After that, the non-adherent cells were harvested, counted and replated at cells (3×10^6) in complete medium (10 mL), and cultured for another 6 days. The

resulting DCs (day 14) was used for further DC maturation assays and in vitro T cell activation assays.

For DC maturation, the obtained immature GM-CSF BMDCs or $CD103^+$ BMDCs (2×10^5 cells per sample) were treated with different vaccines of a certain concentrations in culture medium for 24 hours. The cells were collected by centrifuge at 1500 rpm for 5 min. After being washed with PBS, the cells were incubated with antibodies of CD11c-APC, CD80-FITC, CD40-PE and MHC II-PerCP (BD Biosciences, the antibodies were used according to the manufacturer introduction) in PBA on ice for 15 min. Then, the cells were washed with PBS twice and resuspended in PBS for flow cytometry assay. In addition, the supernatant of the cells after incubation with different vaccines was used to test the IL-12 secretion with Mouse IL-12 (p70) ELISA PRO kit (Mabtech).

4.7 *In vitro* activation of OT-I T cells and DN32.D3 cells

$CD8^+$ T cells harvested from OT-I transgenic mice (termed as OT-I T cells) were isolated by negative selection with $CD8^+$ T-cell isolation kit II (Miltenyi) according to the manufacturer protocol. Sorted cells were stained with CFSE (Thermo Fisher, 2.5 μM) and used directly with no need for further culture.

For *in vitro* activation of OT-I T cells, $CD103^+$ BMDCs (10^4 cells per sample) from day 14 were incubated with different vaccines at different concentrations at 37 °C with 5% CO_2 for 24 hours. Subsequently, CFSE-labeled OT-I T cells ($5x10^4$) were added and co-cultured for 72 hours. Proliferation of OT-I T cells was assessed by flow cytometry (BD FACSCalibur). The calculation of the Mean cycle was obtained as described by Valente *et al.*[35] Generally, the CFSE dilution factor (f) was calculated by dividing the stimulated mean fluorescence intensity (MFI) with the unstimulated MFI. Then, the mean cycle was calculated

with the formula of "Log2(f)". In addition, the secretion of two critical cytokines, IFNɤ and IL2, were analyzed with ELISA assay (Mabtech).

For *in vitro* activation of DN32.D3 NKT cell hybridoma's, $CD103^+$ BMDCs ($5x10^4$ cells per sample) from day 14 were incubated with the OVA-αGalcer nanovaccines and the soluble controls (OVA+ αGalcer) at different concentrations at 37 °C with 5% CO_2 for 3 hours. Subsequently, DN32.D3 cells ($1x10^5$ cells) were added and co-cultured for 24 hours. The supernatant was collected to perform IL2 ELISA.

4.8 *In vivo* activation of OT-I T cells

For *in vivo* activation of OT-I T cells, Celltrace violet (Life technologies)-labelled OT-I T cells (3×10^6) were adoptively transferred into C57BL/6 mice by intravenous injection. The following day, mice were vaccinated with NP-pHLIPs, NP-ctrls or soluble OVA+LPS at a dose of OVA corresponding to 0.5 μg. Three days later, the mice were sacrificed and spleens were harvested. Splenocyte suspension was obtained after organ mechanical disruption and cells were passed through 100 μm cell strainer (Falcon). A FITC-tagged CD8 antibody (BD Biosciences) was used to label OT-I T cells. Proliferations of OT-I T cells were evaluated by dilution of Celltrace violet intensity with flow cytometry (FACS verse BD Biosciences).

4.9 *In vitro* activation of NY-ESO-1 specific T cells

$CD14^+$ monocytes and naïve $CD8^+$ T cells were isolated from HLA-A2 typed healthy donors buffy coat respectively with CD14 Microbeads and naïve $CD8^+$ T cell isolation kit (Miltenyi). Sorted cells were stored in liquid nitrogen frozen with 10% DMSO plus 90% FBS until use. $CD14^+$ monocytes were cultured with IL-4 (0.3 U/mL) and GM-CSF (0.45 U/mL) for 6 days in complete RPMI medium. Floating cells were collected and used as moDCs in coculture. mRNA encoding for a TCR specific for HLA-A2-NY-ESO-I peptide (SLLMWITQC)[44] was kindly provided by Ugur Sahin lab. Naïve $CD8^+$ T cells were thawed and electroporated with

mRNA (10 μg) in 4-mm cuvette with one electronic pulse (500mV). Electroporated T cells (5×10^5) were cultured with moDCs (2×10^5) together with soluble NY-ESO-1+LPS, NY-ESO-1/LPS nanoparticles, or polyphenol-coated NY-ESO-1/LPS nanoparticles for 48 hours. IFNy levels in culture supernatants were quantified by ELISA.

Supporting Information

Supporting Information is available from the Wiley Online Library or from the author.

Notes

The authors declare no competing financial interest.

Acknowledgements

We thank the Ludwig Institute for Cancer Research for providing the recombinant NY-ESO-1 protein used in the study. mRNA encoding for a TCR specific for HLA-A2-NY-ESO-I peptide p157–165 was kindly provided by Prof. U. Sahin. This work was supported by the National Key Scientific Program of China (Grants 21505039), ERC Advanced grant PATHFINDER (269019) and a Spinoza grant from the Netherlands Organisation for Scientific Research (NWO). C.F. is recipient of Dutch Cancer Society KWO grant 2009-4402. M.V. is recipient of ERC Starting grant CHEMCHECK (679921) and a Gravity Program Institute for Chemical Immunology tenure track grant by NWO. E.J. received a Czech Academy of Sciences grant (MSM200501602).

References

[1] C.A. Klebanoff, L. Gattinoni, P. Torabi-Parizi, K. Kerstann, A. R. Cardones, S. E. Finkelstein, D. C. Palmer, P. A. Antony, S. T. Hwang, S. A. Rosenberg, *Proc. Natl. Acad. Sci.* **2005,** *102*, 9571.

[2] N. P. Restifo, M. E. Dudley, S. A.Rosenberg, *Nat. Rev. Immunol.* **2012,** 12, 269.

[3] K. Palucka, J. Banchereau, In *Interaction of Immune and Cancer Cells*, Springer, 2014; 75-89.

[4] S. A. Rosenberg, J. C. Yang, N. P. Restifo, *Nat. Med.* **2004,** *10* , 909.

[5] I. J. M. Vries, D. J. Krooshoop, N. M. Scharenborg, W. J. Lesterhuis, J. H. S. Diepstra, G. N. Muijen, S. P. Strijk, T. J. Ruers, O. C. Boerman, W. J. Oyen, *Cancer Res.* **2003,** 63, 12.

[6] P. J. Tacken, I. J. M. Vries, R. Torensma, C. G. Figdor, *Nat. Rev. Immunol.* **2007,** *7*, 790.

[7] G. Zhu, F. Zhang, Q. Ni, G. Niu, X. Chen, *ACS nano* **2017**, *11*, 2387.

[8] S. Hamdy, O. Molavi, Z. Ma, A. Haddadi, A. Alshamsan, Z. Gobti, S. Elhasi, J. Samuel, A. Lavasanifar, *Vaccine* **2008**, *26*, 5046.

[9] Y. Perrie, A. R. Mohammed, D. J. Kirby, S. E. McNeil, V. W. Bramwell, *Int. J. Pharm.* **2008,** *364*, 272.

[10] J. Kazzaz, M. Singh, M. Ugozzoli, J. Chesko, E. Soenawan, D. T. O'Hagan, *J. Control. Release* **2006**, *110*, 566.

[11] S. Hamdy, A. Haddadi, R. W. Hung, A. Lavasanifar, Adv. Drug Deliv. Rev. **2011**, *63*, 943.

[12] A. Saupe, W. McBurney, T. Rades, S. Hook, *Expert Opin Drug Deliv.* **2006**, *3*, 345.

[13] S. D. Xiang, K. Scalzo-Inguanti, G. Minigo, A. Park, C. L. Hardy and M. Plebanski, *Expert Rev Vaccines* **2008**, *7*, 1103.

[14] O. P. Joffre, E. Segura, A. Savina and S. Amigorena, *Nat. Rev. Immunol.* **2012**, *12*, 557.

[15] W. R. Heath, G. T. Belz, G. Behrens, C. M. Smith, S. P. Forehan, I. A. Parish, G. M. Davey, N. S. Wilson, F. R. Carbone and J. A. Villadangos, *Immunol. Rev.* **2004**, *199*, 9.

[16] Q. Fu, J. Sun, W. Zhang, X. Sui, Z. Yan and Z. He, *Recent Pat Anticancer Drug Discov.* **2009**, *4*, 262.

[17] W. J. Gradishar, *Expert Opin Pharmacother,* **2006**, *7*, 1041.

[18] Q. Chen, X. Liu, J. Zeng, Z. Cheng and Z. Liu, *Biomaterials*, **2016**, *98*, 23.

[19] T. S. Sileika, D. G. Barrett, R. Zhang, K. H. A. Lau and P. B. Messersmith, *Angew. Chem. Int. Ed.* **2013**, *52*, 10766.

[20] M. An, D. Wijesinghe, O. A. Andreev, Y. K. Reshetnyak and D. M. Engelman, *Proc. Natl. Acad. Sci.* **2010**, *107*, 20246.

[21] D. Weerakkody, A. Moshnikova, M. S. Thakur, V. Moshnikova, J. Daniels, D. M. Engelman, O. A. Andreev and Y. K. Reshetnyak, *Proc. Natl. Acad. Sci.* **2013**, *110*, 5834.

[22] A. P. Rapoport, E. A. Stadtmauer, G. K. Binder-Scholl, O. Goloubeva, D. T. Vogl, S. F. Lacey, A. Z. Badros, A. Garfall, B. Weiss and J. Finklestein, *Nat. Med.* **2015**, *21*, 914.

[23] S. Rahimian, J. W. Kleinovink, M. F. Fransen, L. Mezzanotte, H. Gold, P. Wisse, H. Overkleeft, M. Amidi, W. Jiskoot and C. W. Löwik, *Biomaterials*, **2015**, *37*, 469.

[24] Y. Dölen, M. Kreutz, U. Gileadi, J. Tel, A. Vasaturo, E. A. van Dinther, M. A. van Hout-Kuijer, V. Cerundolo and C. G. Figdor, *Oncoimmunology*, **2016**, *5*, e1068493.

[25] J. T. Ulrich and K. R. Myers, *in Vaccine design, Springer*, **1995**,495.

[26] S. Quideau, D. Deffieux, C. Douat-Casassus and L. Pouysegu, *Angew. Chem. Int. Ed.* **2011**, *50*, 586.

[27] C. S. Yang, X. Wang, G. Lu and S. C. Picinich, *Nat. Rev. Cancer*, **2009**, *9*, 429.

[28] J. Li, S. Wu, C. Wu, L. Qiu, G. Zhu, C. Cui, Y. Liu, W. Hou, Y. Wang and L. Zhang, *Nanoscale*, **2016**, *8*, 8600.

[29] M. Gutscher, A.-L. Pauleau, L. Marty, T. Brach, G. H. Wabnitz, Y. Samstag, A. J. Meyer and T. P. Dick, *Nat. meth.* **2008**, *5*, 553.

[30] H. Hemmi, O. Takeuchi, T. Kawai, T. Kaisho, S. Sato, H. Sanjo, M. Matsumoto, K. Hoshino, H. Wagner and K. Takeda, *Nature*, **2000**, *408*, 740.

[31] O. A. Andreev, A. G. Karabadzhak, D. Weerakkody, G. O. Andreev, D. M. Engelman and Y. K. Reshetnyak, *Proc. Natl. Acad. Sci.* **2010**, *107*, 4081.

[32] S. Sang, J. D. Lambert, J. Hong, S. Tian, M.-J. Lee, R. E. Stark, C.-T. Ho and C. S. Yang, *Chem Res Toxicol*, **2005**, *18*, 1762.

[33] S. Baghirova, B. G. Hughes, M. J. Hendzel and R. Schulz, *Methods,* **2015**, *2*, 440.

[34] G. H. Pritchard, E. W. Cross, M. Strobel, S. C. Jameson, R. M. Kedl, K. A. Hogquist and C. A. Hunter, *Nat. Immunol.* **2016**, *17*, 471.

[35] M. Valente, C. Baey, P. Louche, C. A. Dutertre, L. Vimeux, C. Marañón, A. Hosmalin and V. Feuillet, *Eur J Immunol.* **2014**, *44*, 2274.

[36] H. Takayanagi, K. Ogasawara, S. Hida, T. Chiba, S. Murata, K. Sato, A. Takaoka, T. Yokochi, H. Oda and K. Tanaka, **Nature**, *2000*, 408, 600.

[37] Y. Li, X. C. Li, X. X. Zheng, A. D. Wells, L. A. Turka and T. B. Strom, *Nat. Med.* **1999**, *5*, 1298.

[38] Y.-H. Chiu, J. Jayawardena, A. Weiss, D. Lee, S.-H. Park, A. Dautry-Varsat and A. Bendelac, *J. Exp. Med.* **1999**, *189*, 103.

[39] J. Yuan, M. Adamow, B. A. Ginsberg, T. S. Rasalan, E. Ritter, H. F. Gallardo, Y. Xu, E. Pogoriler, S. L. Terzulli and D. Kuk, *Proc. Natl. Acad. Sci.*, **2011**, *108*, 16723.

[40] A. Wadle, A. Mischo, S. Strahl, H. Nishikawa, G. Held, F. Neumann, B. Wullner, E. Fischer, S. Kleber and J. Karbach, *Yeast*, **2010**, *27*, 919.

[41] M. B. Lutz, N. Kukutsch, A. L. Ogilvie, S. Rößner, F. Koch, N. Romani and G. Schuler, *J. Immunol. meth.* **1999**, *223*, 77.

[42] Y. Xu, Y. Zhan, A. M. Lew, S. H. Naik and M. H. Kershaw, *J. Immunol.* **2007**, *179*, 7577.

[43] L. van de Laar and B. N. Lambrecht, *Blood*, **2014**, *124*, 3036.

[44] D. A. Schmid, M. B. Irving, V. Posevitz, M. Hebeisen, A. Posevitz-Fejfar, J. F. Sarria, R. Gomez-Eerland, M. Thome, T. N. Schumacher and P. Romero, *J. Immunol.* **2010**, *184*, 4936.

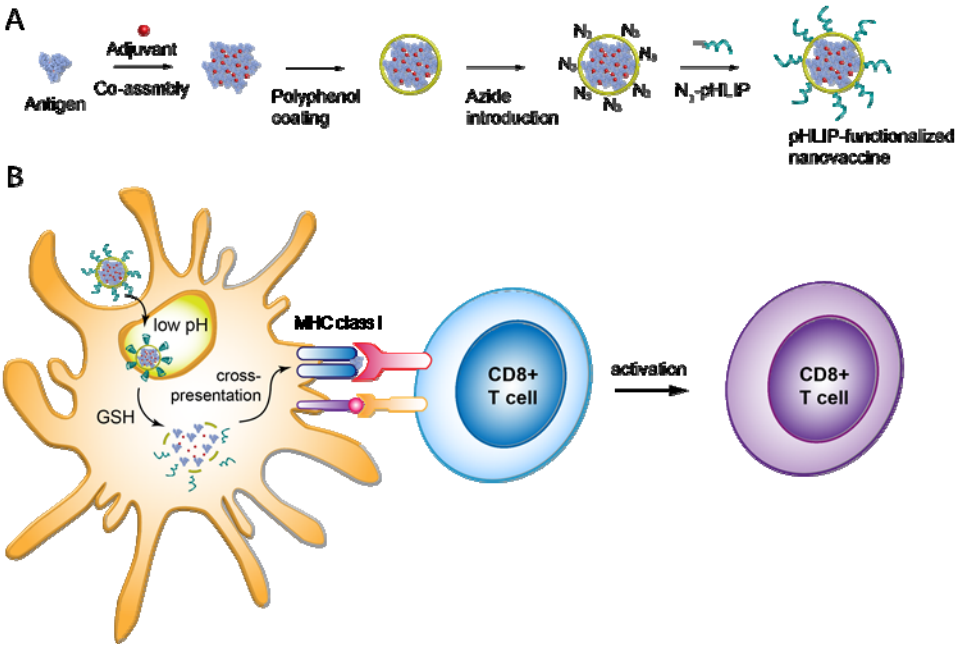

Figure 1. (A) **Synthesis of the pHLIP-functionalized nanovaccine.** Addition of immunostimulatory adjuvant can induce antigen assembly into nanoparticles. The antigen-adjuvant nanoparticles were coated with polyphenol and then incorporated with azide groups. Finally, alkyne-tagged pHLIP was installed onto the surface of the polyphenol-coated nanovaccine through copper-catalyzed azide-alkyne Huisgen cycloaddition. (B) **Working principle of the pHLIP-functionalized nanovaccine for enhanced cytotoxic $CD8^+$ T cell activation.** The nanovaccine was first endocytosed by DCs, and then escaped from the low-pH endolysosome into cytosol via the pH-sensitive membrane translocation capability of pHLIP. Subsequently, the polyphenol coating was degraded by cytoplasmic GSH, facilitating the release of the antigen cargo to enhance their cross-presentation, which is expected to enhance cytotoxic T cell activation.

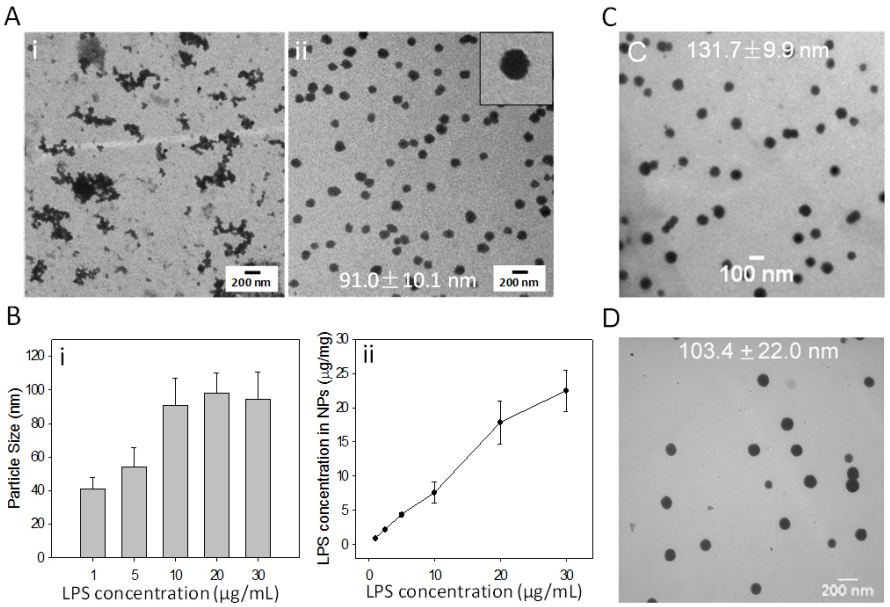

Figure 2. Adjuvant-induced antigen assembly. (A) TEM images of OVA only (i) and OVA-LPS nanoparticles (ii). The concentration of OVA and LPS was 1 mg/mL and 10 μg/mL, respectively. (B) Optimization of the OVA-LPS nanoparticle formulation by assessing the particle size (i) and the LPS loading amount (ii). The OVA concentration was fixed at 1 mg/mL. Error bars represent the standard deviation of three independent experiments. (C) TEM images of OVA-α-Galcer nanoparticles. (D) TEM images of OVA-MPLA nanoparticles.

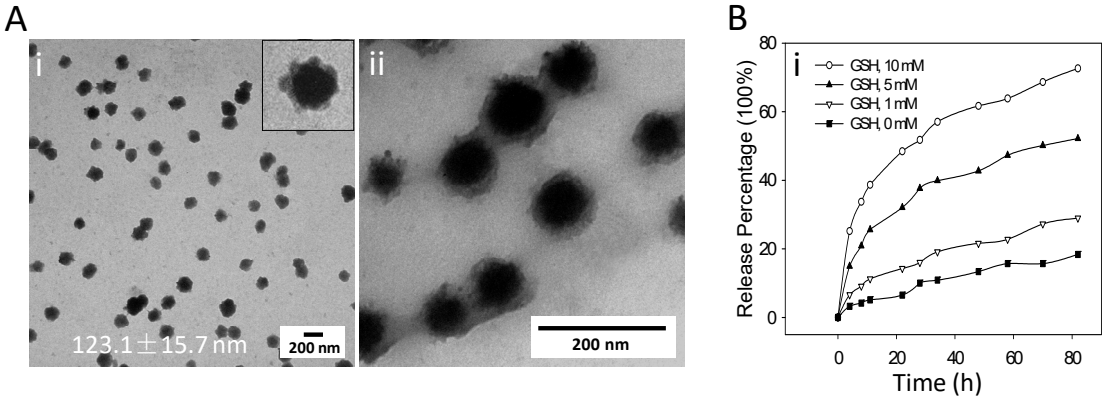

Figure 3. Polyphenol coating of the OVA-LPS nanoparticles. (A) TEM of OVA-LPS nanoparticles coated with polyphenol for 1 hour (i, ii). To observe the structure details, a large

imaging scale was applied in Panel ii; (B) Release kinetic profiles of the ATTO-647 dye incorporated into the OVA-LPS nanoparticles, which were coated with polyphenol for 1 hour, in PBS containing GSH of different concentrations.

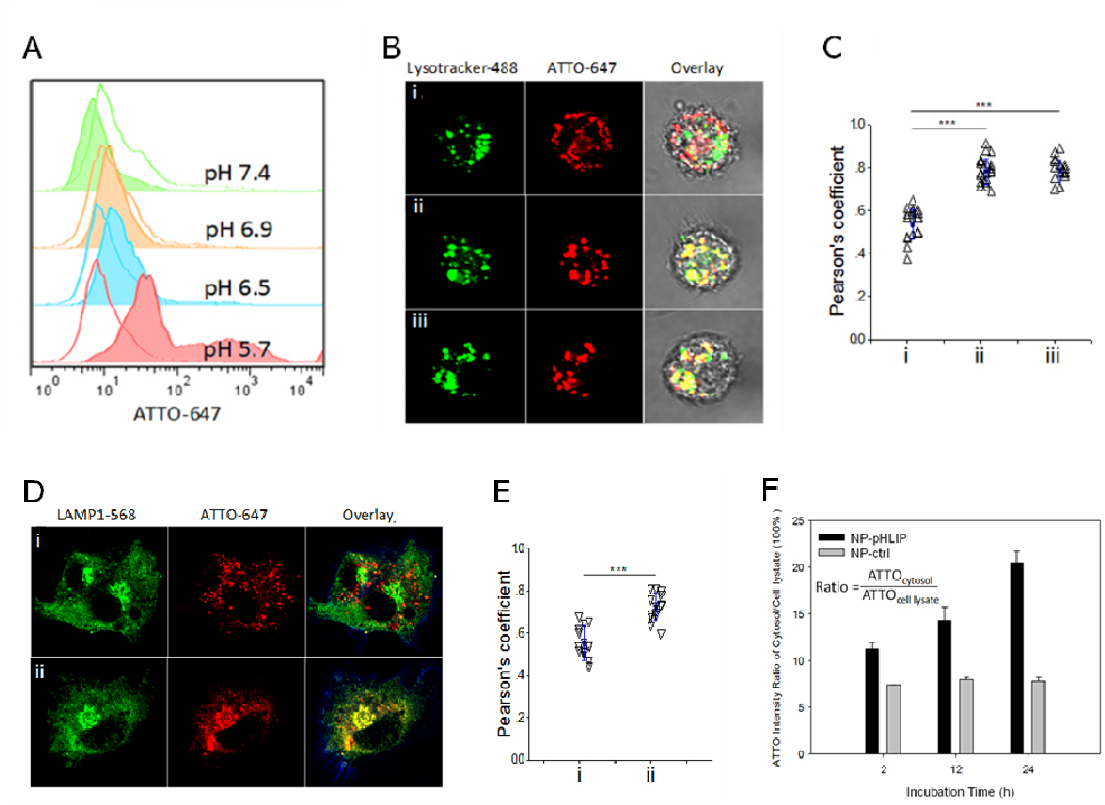

Figure 4. Cell uptake and intracellular distribution of different nanovaccines. (A) Flow cytometry assay of DCs incubated with NP-ctrls (line) and NP-pHLIPs (solid) in phosphate buffer of different pH value for 1 hour. (B) CLSM images of JAWSII cells incubated with NP-pHLIPs (i), NP-ctrls (ii) or NPs (iii) in culture medium (pH 7.4) for 7 h, and then stained with lysotracker-488. (C) Corresponding colocalization of lysotracker-488 and NP derived ATTO-647 in B as Pearson's coefficient. (D) CLSM images of JAWSII cells incubated with NP-pHLIPs (i) or NP-ctrls (ii) in culture medium (pH 7.4) for 7 h, fixed, and then stained with primary antibody and fluorescent secondary antibody of LAMP1. (E) Corresponding colocalization of LAMP1 with NP derived ATTO-647 in D as Pearson's coefficient. One data point (triangle) in both Figure 4C and 4E represents one Pearson's Coefficient obtained from

individual CLSM image. Six to seven images were recorded for each sample group, and three independent experiments were performed, ***P < 0.001 by Student's *t*-test. (F) The OVA-ATTO-647 content in cytosol. Error bars represent the standard deviation of three independent experiments.

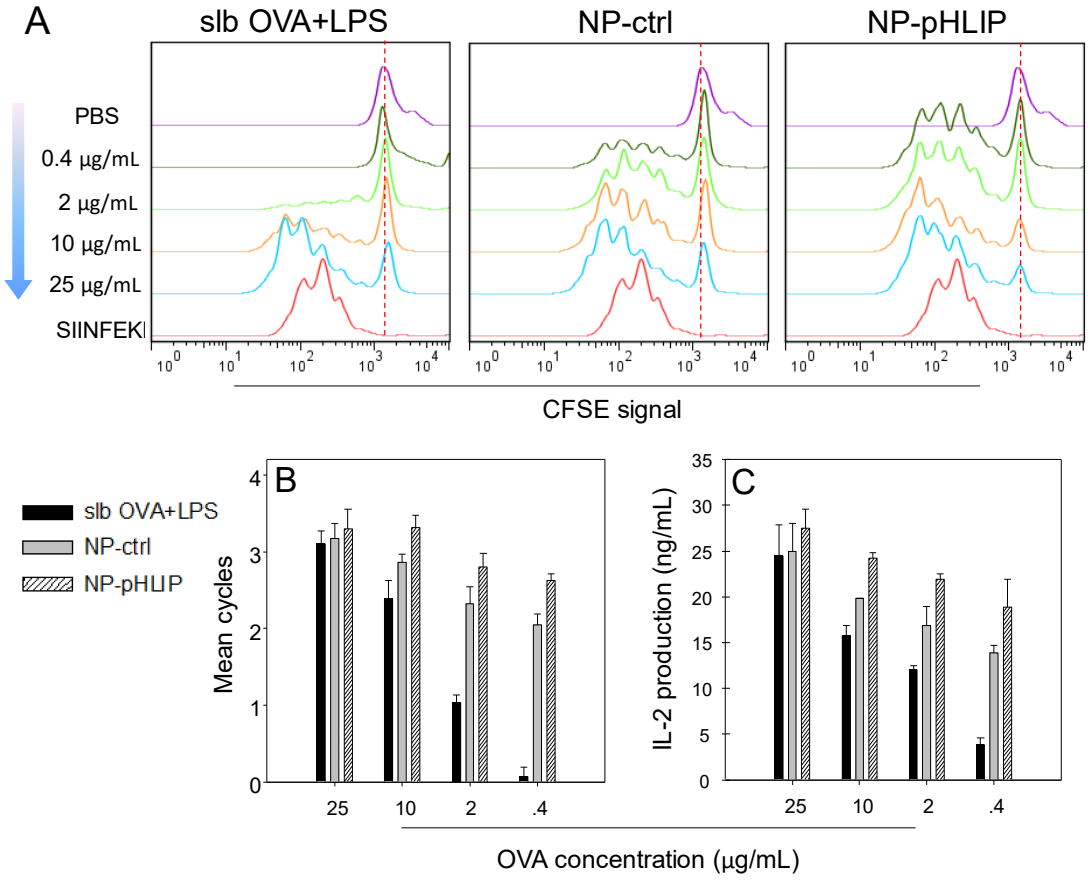

Figure 5. *In vitro* cross-presentation of OVA by DCs for priming OT-I T cells. (A) Proliferation assay of CFSE-labeled OT-I T cells after 72-hour incubation with $CD103^{+}$ BMDCs which were pretreated with soluble OVA+LPS, NP-ctrls or NP-pHLIPs for 24 hours. OVA-derived SIINFEKL peptide was used as a positive control. (B) Corresponding mean cell division cycles. (C) Corresponding IL-2 production.

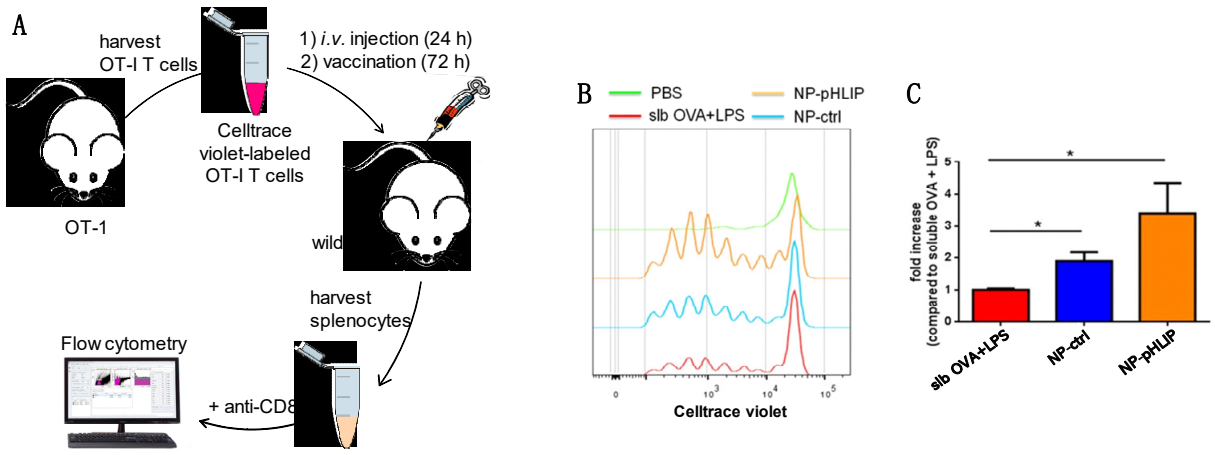

Figure 6. *In vivo* cross-presentation of OVA by splenic DCs for priming OT-1 T cells. (A) Overview of the workflow. OT-I T cells were harvested from OT-I transgenic mice, labelled with Celltrace violet, and then adoptively transferred into C57BL/6 mice by intravenous injection. After 24 hours, the mice were vaccinated with NP-pHLIPs, NP-ctrls or soluble OVA+LPS at a dose of OVA corresponding to 0.5 µg. After 72 hours, the mice were sacrificed and the splenocytes were collected. The OT-1 T cells were stained with a FITC-tagged CD8 antibody and analyzed with flow cytometry. (B) Representative histogram of Celltrace violet signal from transferred OT-I T cells. (C) Fold increase in corresponding mean cycles. Five mice per group were tested, *P < 0.05 by Student's *t*-test.

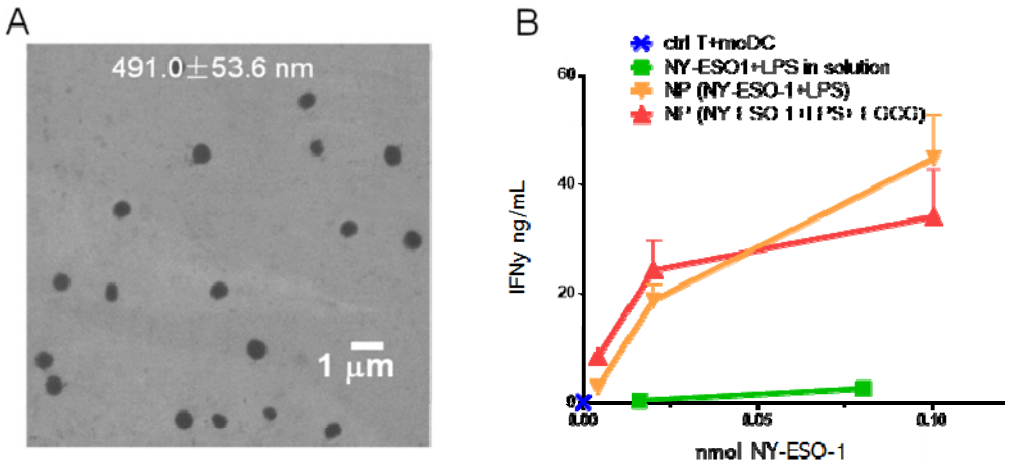

Figure 7. NY-ESO-1-specific cross-priming of cytotoxic T cell. (A) TEM images of NY-ESO-1/LPS nanoparticles. (B) Human monocyte-derived dendritic cells and NY-ESO-1 TcR transfected autologous $CD8^+$ T cells were incubated with either LPS only (blue), soluble NY-ESO-1+LPS (green), NY-ESO-1/LPS nanoparticles (orange) or polyphenol-coated NY-ESO-1/LPS nanoparticles (red). The ability to cross-prime NY-ESO-1-specific cytotoxic T cells was measured by IFNγ secretion.

Supporting Information

Title: Endolysosomal-Escape Nanovaccines through adjuvant-induced tumor antigen assembly for enhanced effector CD8$^+$ T cell activation

Liping Qiu, Michael Valente, Yusuf Dolen, Eliezer Jäger, Martin ter Beest, Liyan Zheng, Carl G. Figdor and Martijn Verdoes**

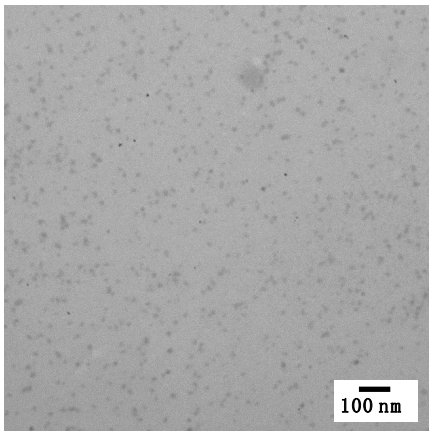

Figure S1. TEM images of the mixture of OVA (I mg) and LPS (10 μg) in PBS without stirring treatment.

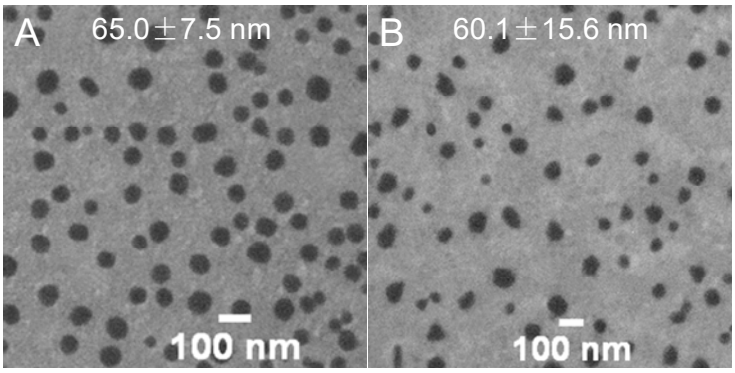

Figure S2. Universality of adjuvant-induced antigen assembly into nanoparticles. TEM images of BSA-LPS nanoparticles (A) and SSA-LPS nanoparticles (B). For preparation of the antigen-adjuvant nanoparticles, BSA or SSA of 1 mg were mixed with LPS of 10 μg in 1 mL PBS under moderate stirring at 4 ^{o}C for 48 hours, respectively.

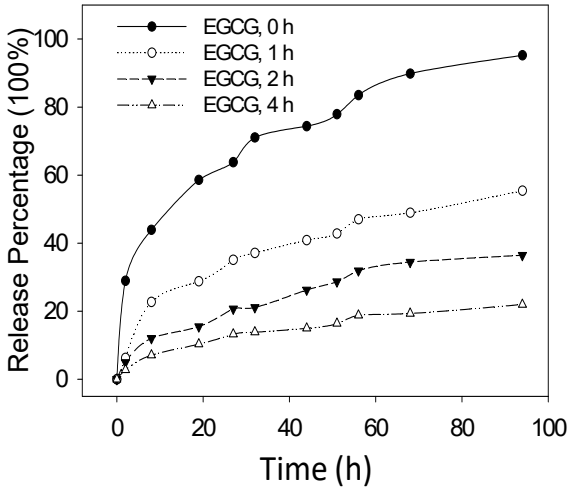

Figure S3. Release kinetic profiles of the ATTO-647 dye incorporated into the OVA-LPS nanoparticles, which were coated with polyphenol for different lengths of time, in PBS containing 5 mM GSH.

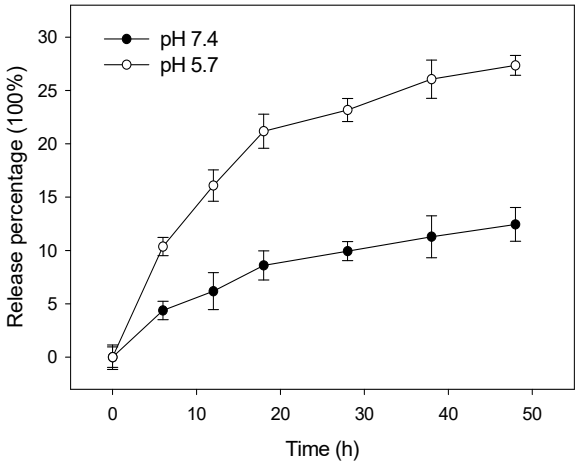

Figure S4. Release kinetic profiles of the ATTO-647 dye incorporated into the OVA-LPS nanoparticles, which were coated with polyphenol for 1 hour, in PBS of two different pH values.

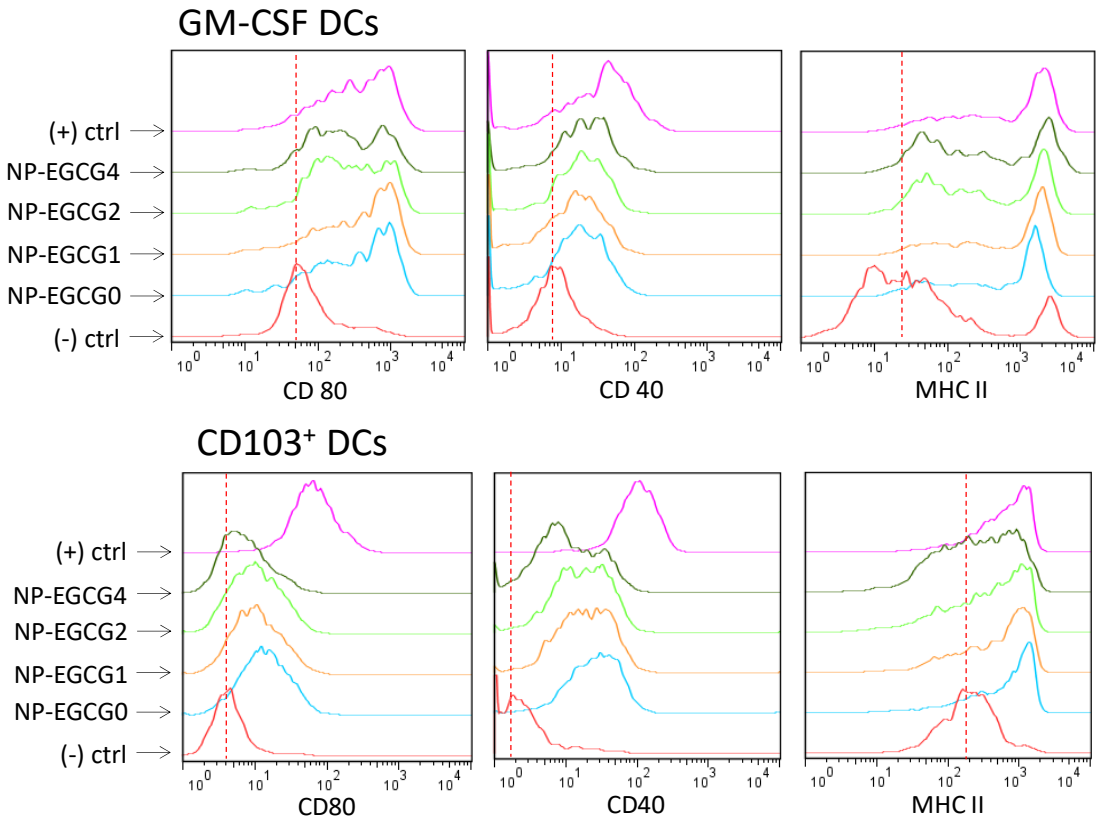

Figure S5. Impact of the polyphenol coating on DC maturation. Two immature BMDC cells (GM-CSF DCs and CD103^{+} DCs) were separately incubated with four OVA-LPS nanoparticles of different polyphenol coating strengths for 24 hours and then analyzed by immunofluorescent flow cytometry. The expression of MHC II and the co-stimulatory molecules CD80 and CD40 were used to assess the maturation state of DCs. "NP-EGCG0/1/2/4" indicates the OVA-LPS nanoparticles which were incubated in the EGCG solution for 0/1/2/4 hours to form a polyphenol coating. Positive control (+ ctrl) and negative control (- ctrl) indicates BMDCs incubated with 10 μg/mL LPS and PBS only for 24 hours, respectively.

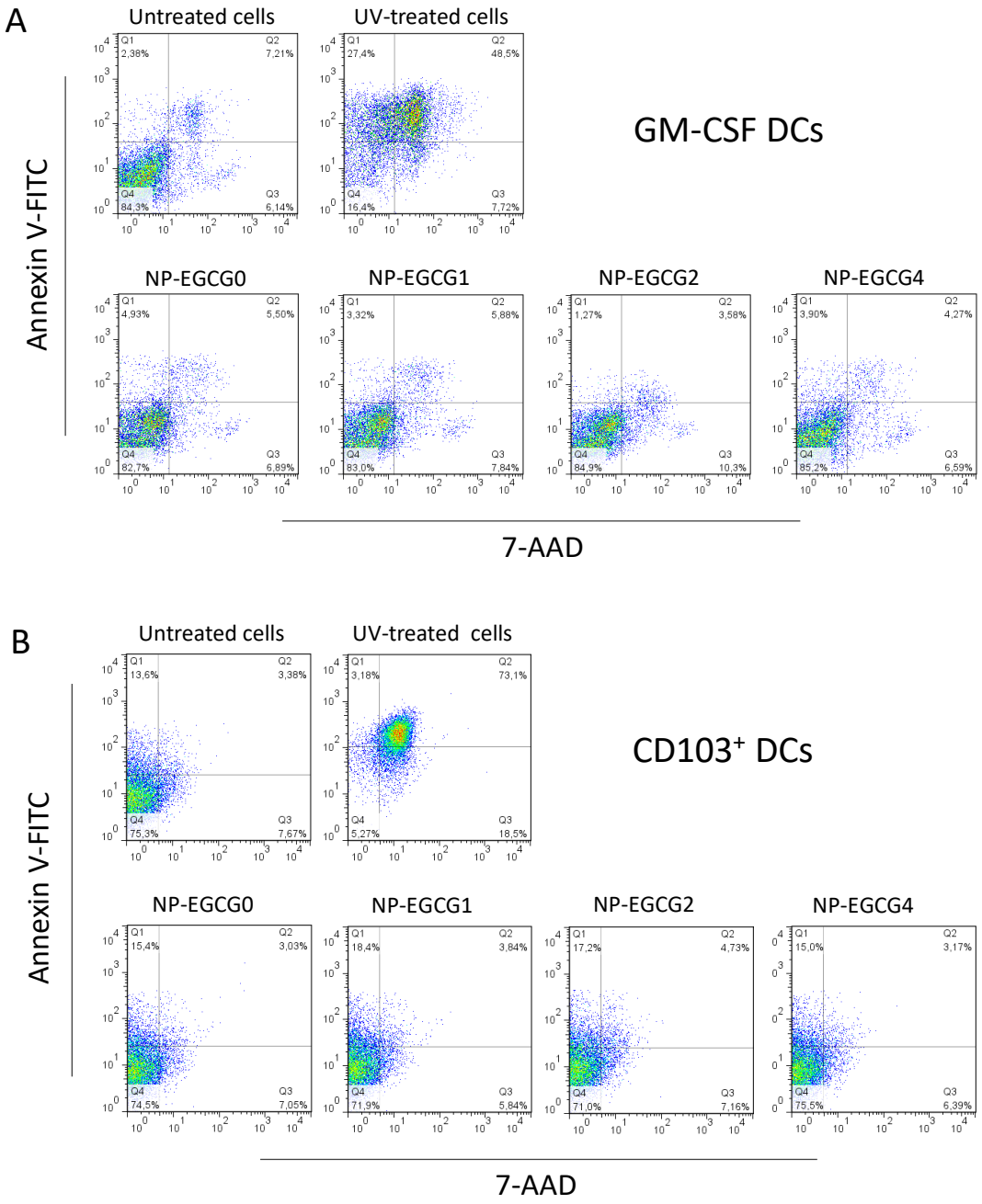

Figure S6. Impact of polyphenol coating on DC viability. GM-CSF BMDCs or $CD103^+$ BMDCs were separately incubated with four OVA-LPS nanoparticles of different polyphenol coating strength for 48 hours and then analyzed with Annexin/7-AAD assays. "NP-EGCG0/1/2/4" indicates the OVA-LPS nanoparticles which were incubated in the EGCG solution for 0/1/2/4 hours to form a polyphenol coating. To prepare the dead cell sample, DCs were irradiated with UV light (254 nm, 8 W) for 10 min and then incubated at 37 ^oC with 5% CO_2 for 48 hours. The nanovaccine concentration of each sample was 100 μg/mL

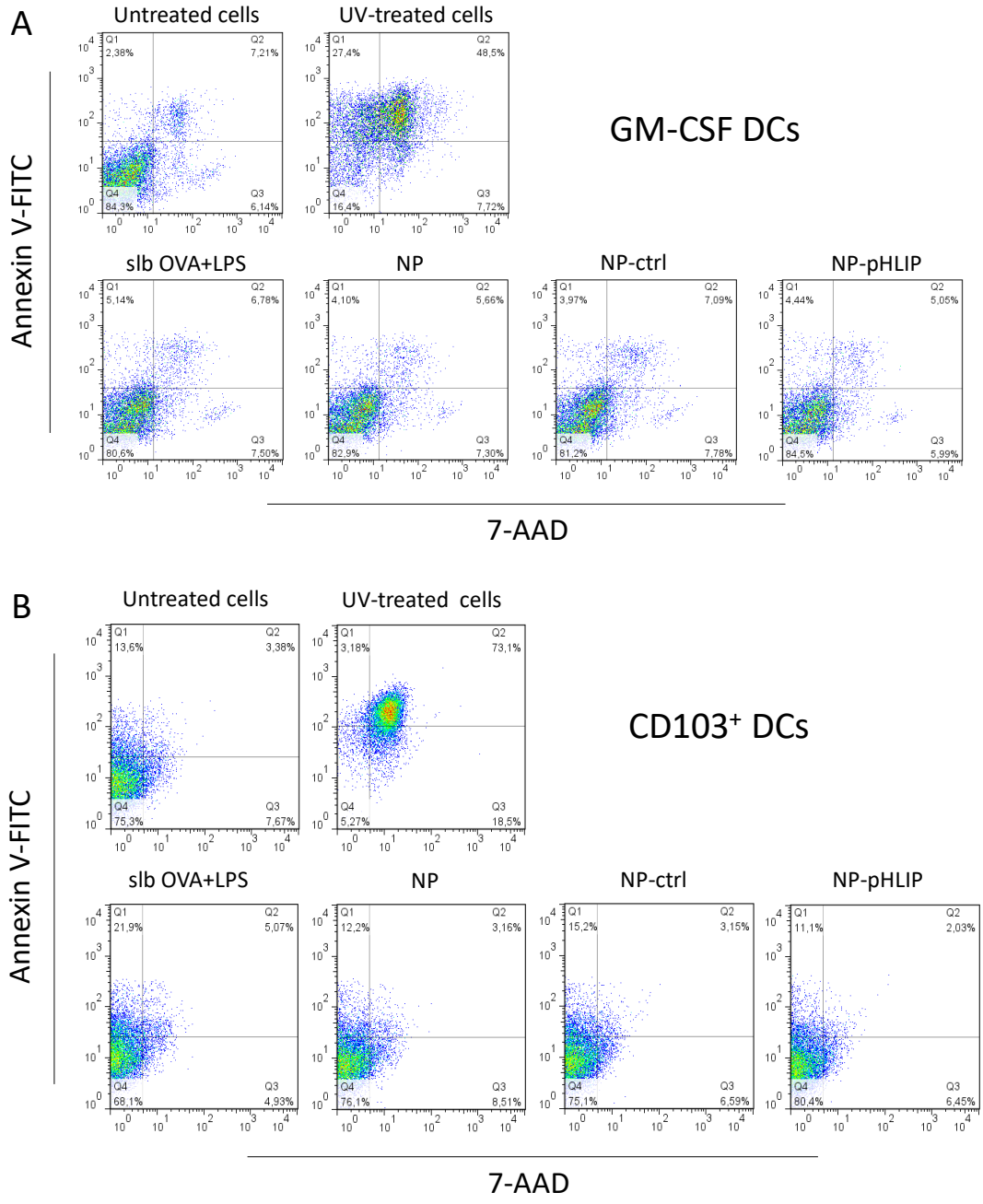

Figure S7. Impact of peptide functionalization on DC viability. GM-CSF BMDCs and CD103^{+} BMDCs were separately incubated with four soluble OVA-LPS, NP, NP-ctrl and NP-pHLIP for 48 hours and then analyzed with Annexin/7-AAD assays. To prepare the dead cell sample, DCs were irradiated with UV light (254 nm, 8 W) for 10 min and then incubated at 37 ^{o}C with 5% CO_2 for 48 hours. The nanovaccine concentration of each sample was 100 μg/mL

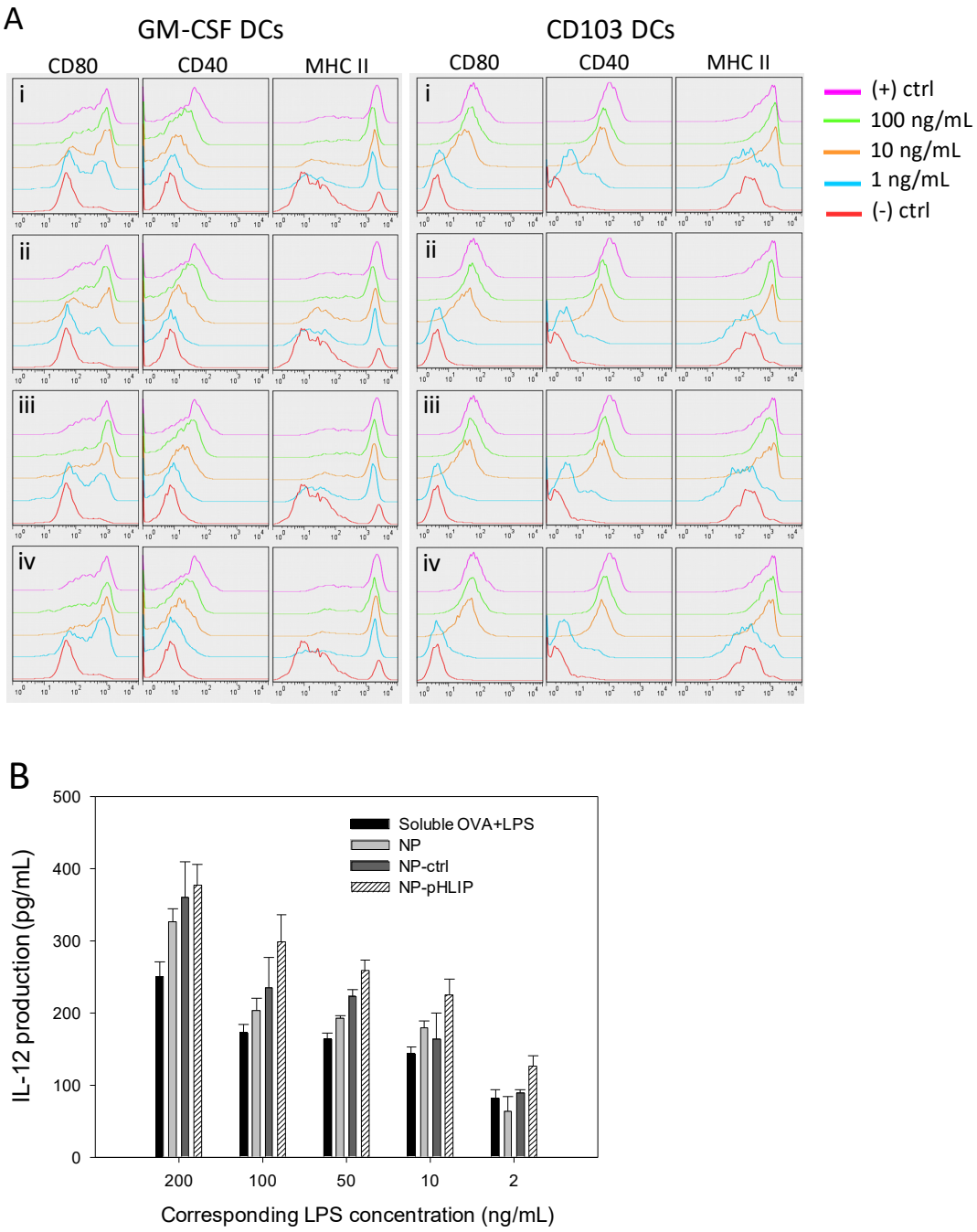

Figure S8 Effect of different vaccines on DC maturation. (A) GM-CSF BMDCs and $CD103^+$ BMDCs were separately incubated with soluble OVA+LPS (i), NPs (ii), NP-ctrls (iii) and NP-pHLIPs (iv) of different concentrations for 24 hours, and then analyzed by flow cytometry. The expression of MHC II and the co-stimulatory molecules CD80 and CD40 were used to assess the maturation state of DCs. Positive control (+ ctrl) and negative control

(- ctrl) indicates BMDCs incubated with 10 μg/mL LPS and PBS only for 24 hours, respectively. (B) Corresponding IL-12 production of GM-CSF DCs after treatment with different vaccines. Error bars represent the standard deviation of three independent experiments.

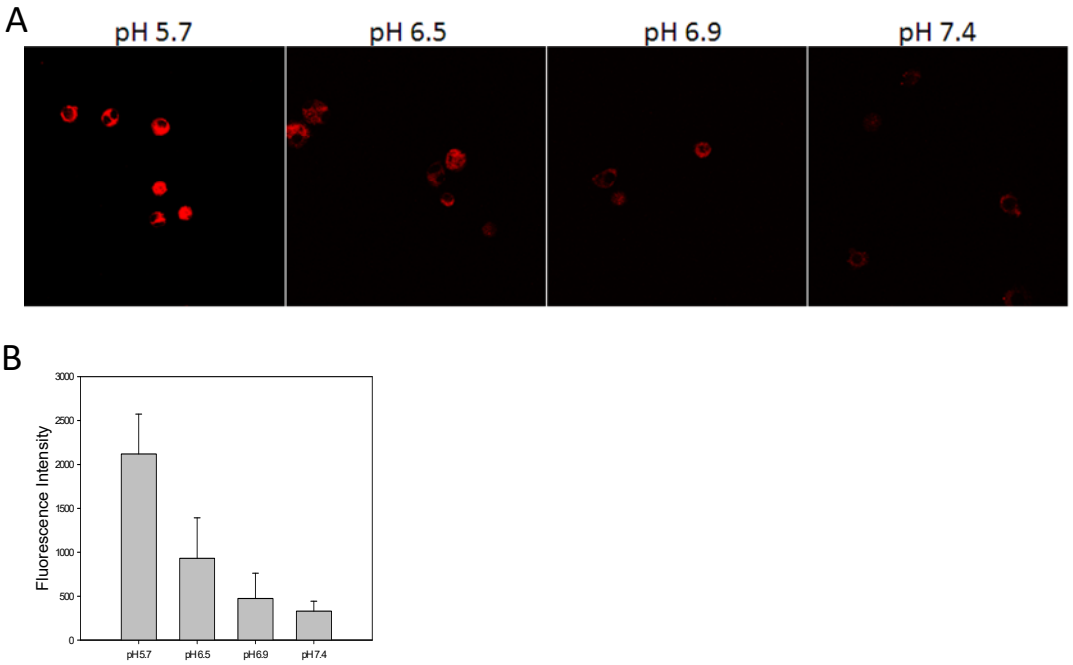

Figure S9. (A) CLSM images of JAWS II cells separately incubated with fluorescent NP-pHLIPs in phosphate buffer solution of pH 5.7, 6.5, 6.9 and 7.4 at 37 ^{o}C with 5% CO_2 for 1 hour; (B) Relative fluorescence intensity of corresponding samples.

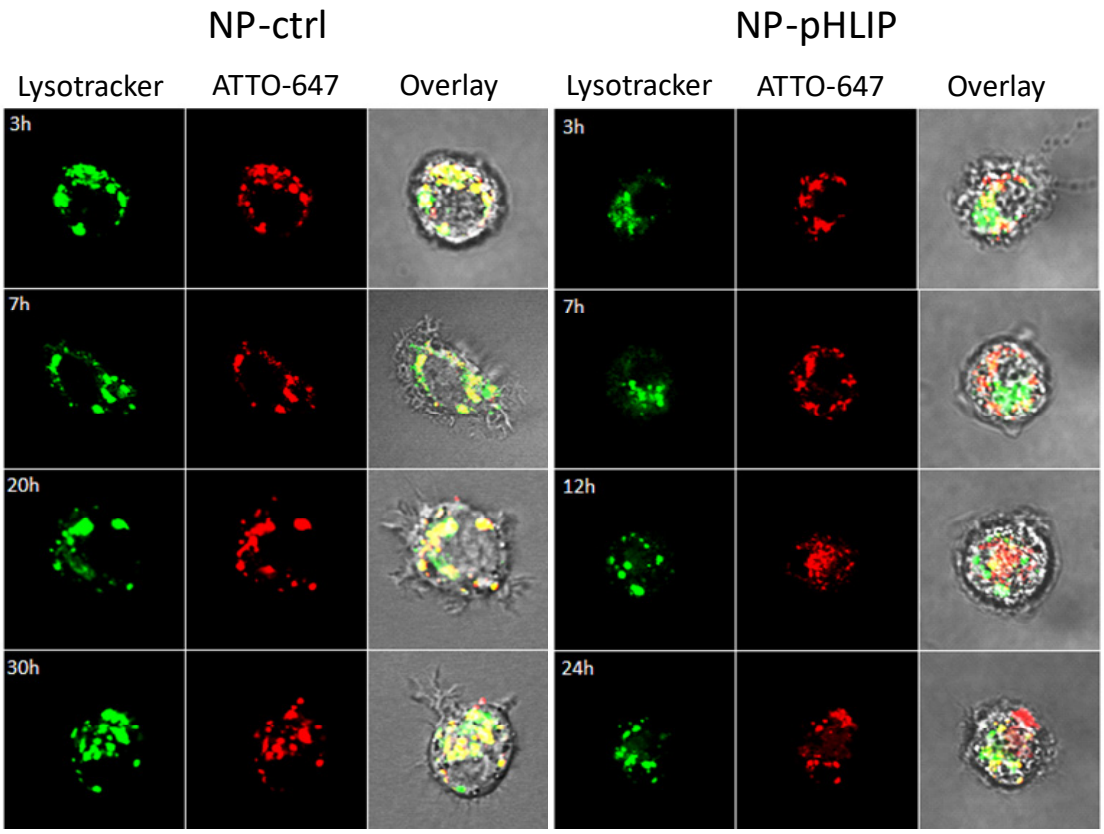

Figure S10. CLSM images of JAWS II cells separately incubated with fluorescent NP-ctrls and NP-pHLIPs in culture medium at 37 ^{o}C with 5% CO_2 for different lengths of time, and then stained with Lysotracker-488 for 10 min.

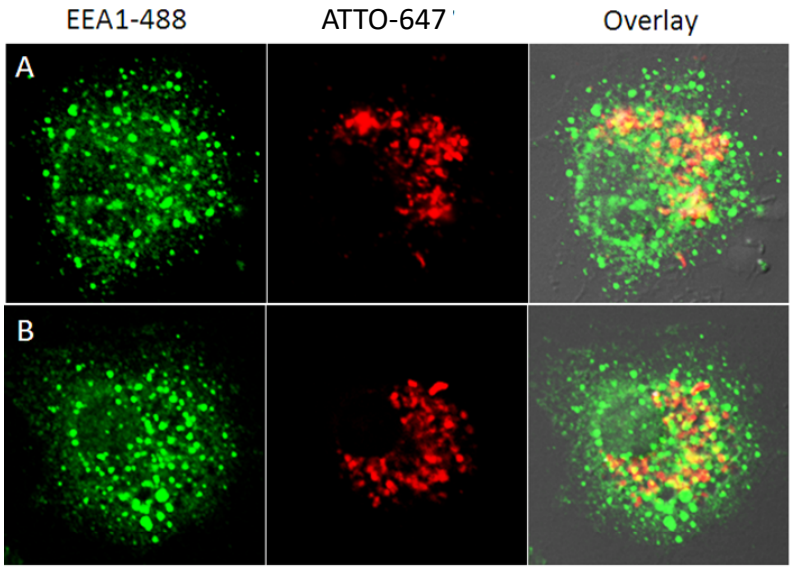

Figure S11. CLSM images of JAWS II cells separately incubated with fluorescent NP-pHLIPs (A) and NP-ctrls (B) in culture medium at 37 ^{o}C with 5% CO_2 for 7 hours, fixed, and then stained with primary antibody and fluorescent secondary antibody of EEA1.

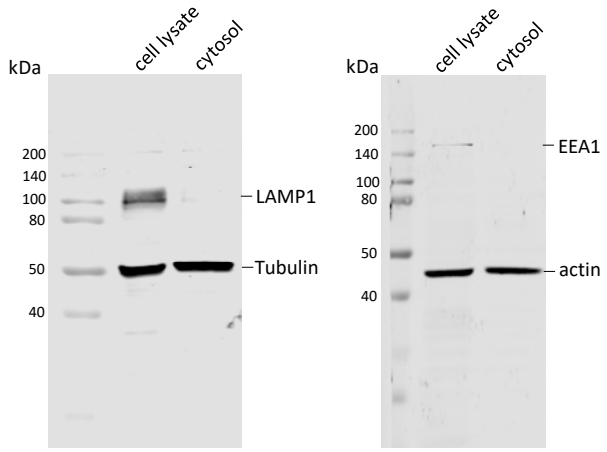

Figure S12. Western blot assay of cytosol and whole cell lysate to verify that the extracted cytosol was free from contaminations of lysosome and endosome.

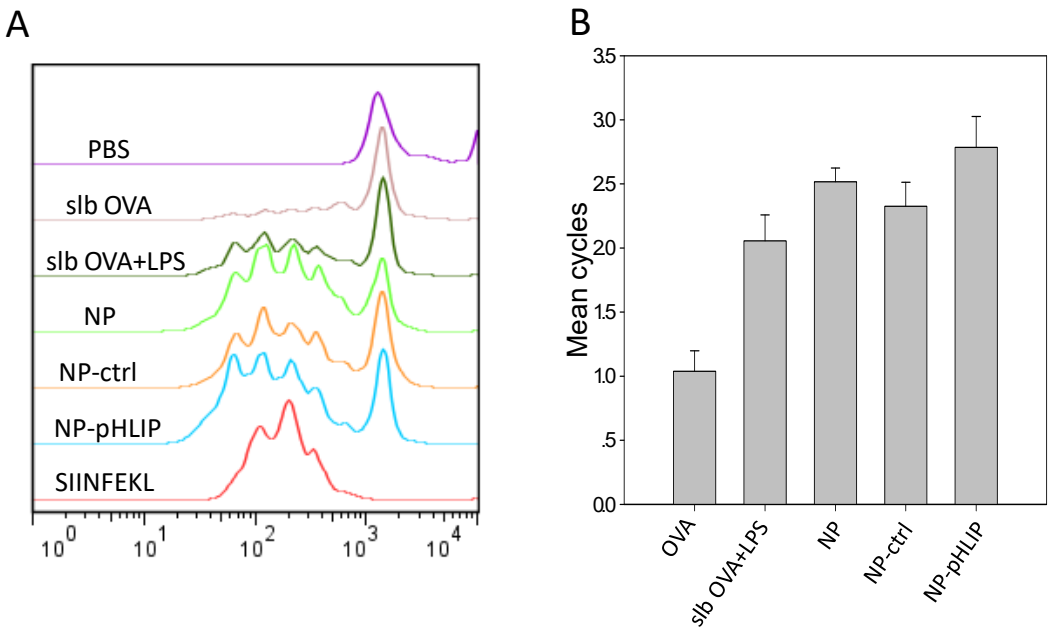

Figure S13. (A) Proliferation assay of CFSE-labeled OT-I T cells after priming with $CD103^+$ BMDCs pulsed with soluble OVA, soluble OVA+LPS, NPs, NP-ctrls and NP-pHLIPs. The OVA concentration of each vaccine was 2 μg/mL. (B) Corresponding mean proliferation cycles.

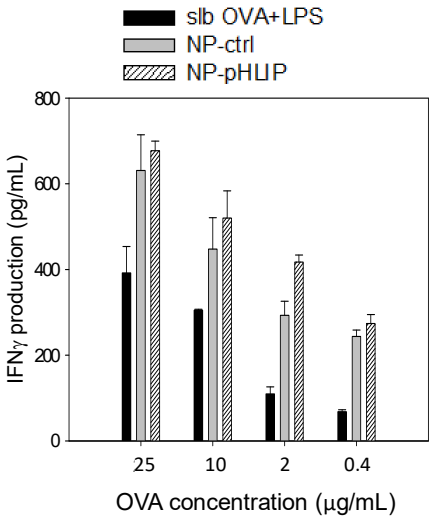

Figure S14. IFNγ production of OT-I T cells after 72-hour incubation with $CD103^{+}$ BMDCs which were pretreated with soluble OVA+LPS, NP-ctrls or NP-pHLIPs for 24 hours. Error bars represent the standard deviation of three independent experiments.

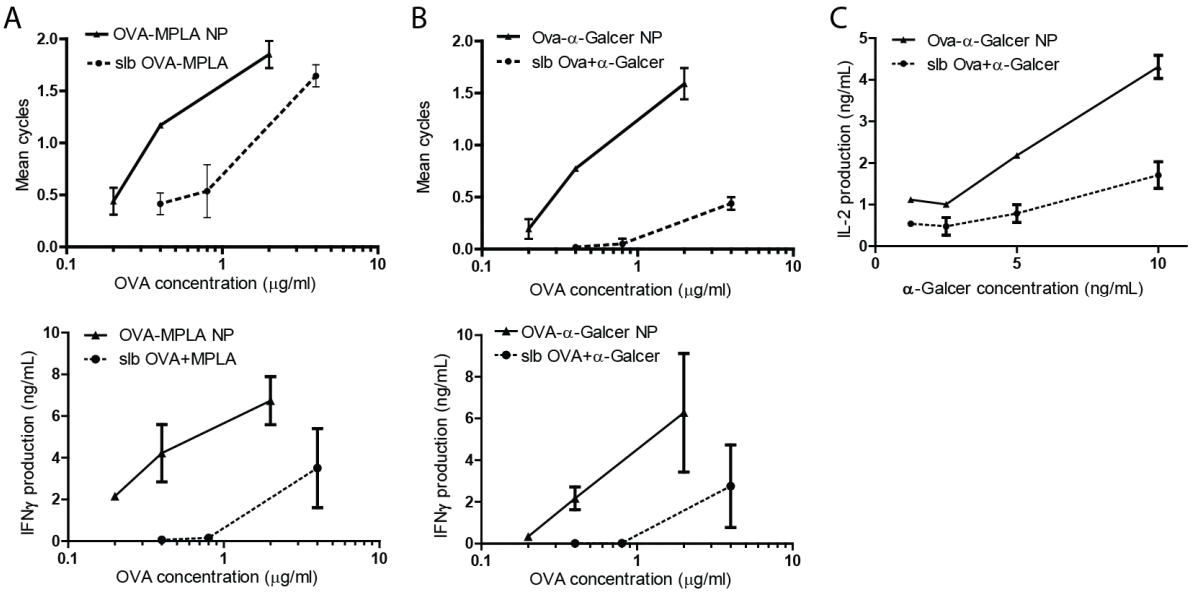

Figure S15. ***In vitro*** **cross-presentation of OVA by DCs for priming OT-I T cells and α-Galcer to** . (A) Proliferation assay (top) and IFNγ production (bottom) of CFSE-labeled OT-I T cells after 72-hour incubation with $CD103^+$ BMDCs which were pretreated with soluble OVA+MPLA or OVA-MPLA NPs for 24 hours. (B) Proliferation assay (top) and IFNγ production (bottom) of CFSE-labeled OT-I T cells after 72-hour incubation with $CD103^+$ BMDCs which were pretreated with soluble OVA+α-GalCer or OVA-α-GalCer NPs for 24 hours. (C) IL-2 response curves of DN32.D3 NKT cell hybridoma cultured 24h with $CD103^+$ BMDCs which were pretreated with soluble OVA+α-GalCer or OVA-α-GalCer NPs.

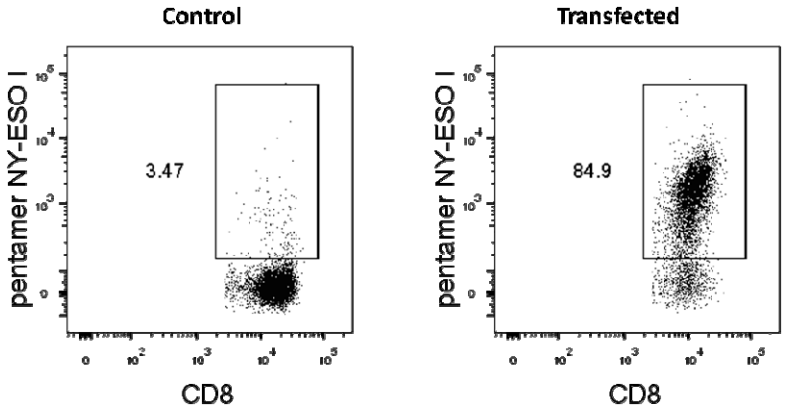

Figure S16. Naïve CD8 T cells were electroporated with 10ug of NY-ESO-I specific TcR mRNA. TcR expression was assessed by flow cytometry 24H post transfection by staining with HLA-A2- SLLMWITQC pentamer and anti-CD8 antibody.